NASA
Technical
Paper
2806

March 1988

p. 32

A Transonic-Small-Disturbance Wing Design Methodology

Pamela S. Phillips,
Edgar G. Waggoner,
and Richard L. Campbell

NASA

NASA Technical Paper 2806

1988

A Transonic-Small-Disturbance Wing Design Methodology

Pamela S. Phillips,
Edgar G. Waggoner,
and Richard L. Campbell

Langley Research Center
Hampton, Virginia

National Aeronautics
and Space Administration

Scientific and Technical Information Division

Summary

An automated transonic design code has been developed which modifies the geometry of a wing from an initial shape in order to obtain a specified pressure distribution. This automated design code utilizes an existing design algorithm which relates changes in surface pressures to changes in the airfoil geometry. The design code iterates between this design algorithm and a three-dimensional transonic-small-disturbance analysis code. In addition to the wing, the analysis portion of the code can model a fuselage, pods, pylons, and a winglet, and this modeling allows the design to take place in a realistic flow environment. A two-dimensional option is also available for airfoil analysis and design.

Several two- and three-dimensional test cases are described to illustrate the capabilities of the automated design code. These test cases include repeats of two previous design efforts which did not use automated computational design. The design test cases were generally successful in that the target pressure distributions were achieved in a reasonable number of design cycles.

Introduction

Recently there has been considerable progress in the development and application of transonic aerodynamic analysis codes. A number of codes have been developed that are capable of computing transonic flow around complex wing-body configurations. One particular analysis code, described in reference 1, solves the transonic-small-disturbance flow equation around a wing-body configuration. This code was later extended to include pods, pylons, winglets, and tails, and thus allows analysis of almost complete aircraft configurations (ref. 2).

One important application of such analysis codes has been the design of airfoils and wings. Some examples of design goals include achieving a maximum lift-drag ratio, a favorable pressure gradient to promote natural laminar flow, or a reduction in the strength of a shock. Depending on the situation, the wing (or airfoil) may be designed from an arbitrary initial shape, or a known shape that exhibits desired characteristics may be refined to achieve the design goals. Typically, a starting shape is analyzed and the results are evaluated to determine what contour changes are needed to satisfy the design requirements. The modified geometry is then analyzed to determine the effectiveness of the modifications. Although this is a cut-and-try approach, it has proven to be a successful design method (refs. 3 and 4). Several design methods have been developed which automate this approach for two-dimensional airfoils and three-dimensional wing sections (refs. 5 to 21). These algorithms have been formulated to eliminate shocks, to design to a specified pressure distribution, or to modify the initial geometry to minimize a specified aerodynamic quantity. An immediate benefit of these automated design procedures is a reduction in man-hours necessary to complete the design. The feasibility of using such computational design methods has increased as the accuracy and reliability of analysis codes have increased.

In this study a transonic wing-airfoil design code has been developed which designs to a specified pressure distribution. A transonic-small-disturbance code (refs. 1 and 2) provides the necessary aerodynamic analysis of the initial and design geometries and allows the design to occur in the presence of a fuselage, pods, pylons, and winglets if desired. Because of the geometric capabilities of the analysis code, more geometrically complex wing design problems can be addressed than was previously possible.

The remainder of this paper is organized in the following manner. A description of the analysis code is presented first, followed by a description of the design algorithm. Results from various two- and three-dimensional design test cases are then shown to demonstrate the capability of the design code. Finally, some comments and recommendations on the use of the design code are included.

Symbols

b	wing span
C_p	pressure coefficient
c	local chord
$f(x,y)$	function defining wing surface
M	Mach number
q	surface velocity
t	iteration count
x,y,z	physical Cartesian coordinates
α	angle of attack
β_0,β_1,β_2	design coefficients
γ	specific heat ratio
Δ	incremental change
η	$2y/b$
ϕ	velocity potential
ω	subsonic relaxation factor
Subscripts:	
i,j,k	indices indicating location of a point in the x-, y-, and z-directions

s	value at surface
x, y, z	partial derivatives with respect to Cartesian coordinates
∞	free stream

Description of the Aerodynamic Analysis Code

The analysis code is described first since many features of the design method are dependent on the structure of the analysis code. The analysis code is the wing, body, pod, pylon, and winglet code of Boppe (refs. 1 and 2), which has been used to analyze a wide variety of configurations. A brief description of the analysis code is presented below with comments focused on a wing-alone configuration. Viscous effects, which may be included in the analysis calculations, are not discussed below. All analysis and design computations performed in this study are inviscid computations. Detailed descriptions of the code are given in references 1 and 2.

The flow equation solved by the code is a nonconservative form of the transonic-small-disturbance approximation to the potential-flow equation:

$$\left[1 - M_\infty^2 - (\gamma+1)M_\infty^2\phi_x - \frac{\gamma-1}{2}M_\infty^2\phi_x^2\right]\phi_{xx} - 2M_\infty^2\phi_y\phi_{xy} + \left[1-(\gamma-1)M_\infty^2\phi_x\right]\phi_{yy} + \phi_{zz} = 0 \tag{1}$$

The classic small-disturbance equation is extended by retaining the term $\phi_x^2\phi_{xx}$ to better approximate the velocity where the flow equation changes from elliptic to hyperbolic type. The terms $\phi_y\phi_{xy}$ and $\phi_x\phi_{yy}$ have also been retained to improve the resolution of swept shocks. The solution is obtained by successive line overrelaxation (SLOR) on an embedded Cartesian grid system through the use of finite-difference techniques. A global, or crude, grid encompasses the entire flow field and extends to infinity in all directions except in the y-direction, where symmetry about the x-z plane at $y = 0$ is assumed. Fine grids may be embedded in the global grid in regions of interest, such as around the wing, body, pod, pylon, and/or winglet (fig. 1). After an initial solution has been obtained on the crude grid (typically after 80 to 100 iterations), a series of iterations are performed that alternate between the crude grid and the fine grid. The number of crude-fine iterations needed to obtain a converged solution varies between 200 and 600 depending upon the configuration and flow conditions.

The crude grid in the x-direction is made up of 51 grid lines. Thirty-eight evenly spaced grid lines traverse the wing from the most forward portion to the most aft portion. Two tangent functions are used to stretch the remaining grid lines to upstream and downstream infinities. A portion of the crude grid is shown in figure 2. A tangent function is also used to generate the grid lines from the wing plane to plus and minus infinity in the z-direction. In the spanwise direction an exponential function generates the grid lines such that 18 lie on the wing, with the wing tip located midway between the 18th and 19th grid lines. It is along these 18 grid lines that the wing fine grids are positioned (fig. 3). The boundary conditions for the symmetry plane are

$$\left.\begin{aligned}\phi_y &= 0\\ \phi_{xy} &= 0\end{aligned}\right\} \tag{2}$$

and for downstream infinity

$$\phi_{yy} + \phi_{zz} = 0 \tag{3}$$

is enforced. The potentials for the remaining crude-grid boundaries are set to zero.

The wing fine grids are evenly spaced in the chordwise and z-directions. Grid points are located at every 1-percent-chord point beginning at 0.5 percent of the chord. This location of the grid points results in the leading and trailing edges being positioned between grid points. The extent of these fine grids in the vertical direction can be determined by the user but is typically 30 percent of the average wing chord above the wing and 10 percent below the wing. The wing fine grids extend 20 percent of the local chord in front of the wing and 10 percent behind it in the streamwise direction. The potentials along this outer boundary are determined by linear interpolation from the previous crude-grid solution and are held fixed. Neumann boundary conditions are applied at the wing plane to form an inner boundary. Once the wing fine-grid potentials are relaxed, linear interpolation is used to compute crude-grid boundary points from fine-grid boundary points at the wing plane. These potentials then become Dirichlet boundary conditions for the crude-grid inner boundary.

The wing is modeled along a constant-z plane with double-valued potentials corresponding to the upper and lower surfaces of each wing section. Information concerning the shape of each wing section is transferred through the inviscid wing boundary conditions

$$\phi_z = f_x - \alpha \tag{4}$$

where $f(x, y)$ defines the wing surface.

Input to this analysis code includes the flow conditions (Mach number and angle of attack), wing planform definition, and wing section definitions. Spanwise and chordwise interpolations are performed on the input geometry to determine the 18 computational wing sections.

Description of Design Method

The design method modifies a specified airfoil or wing geometry until a target pressure distribution is obtained. The design algorithm used in this method was developed by McFadden. (See ref. 13.) It determines the magnitude and direction of the changes to the wing (or airfoil) sections. The premise behind this algorithm is that at a given point the difference between the square of the target surface velocities and the square of the calculated surface velocities is proportional to a change in the surface ordinates. This equation can be expressed as

$$q^2_{\text{target}} - q^2_{\text{calculated}} = \beta_0 \frac{\partial (z_s/c)}{\partial t} \tag{5}$$

where t is the iteration count and β_0 is the proportionality constant. All changes made to the geometry are normal to the wing plane. (See fig. 4.)

Two additional terms are added to this equation to obtain smooth design convergence. The impetus for selecting these two particular terms comes from the work of Davis (ref. 22). Davis observed that relationships between the surface pressure coefficient and the first or second derivative of the surface (depending upon the free-stream Mach number) can be derived from small-disturbance solutions to the wavy-wall problem (ref. 23). The resulting relationships are

$$C_p = \frac{2 \partial z_s/\partial x}{(M^2_\infty - 1)^{1/2}}$$

for supersonic flow, and (6)

$$C_p = \frac{\ell}{\pi} \frac{\partial^2 z_s/\partial x^2}{(1 - M^2_\infty)^{1/2}}$$

for subsonic flow, where ℓ is the wavelength of the undulations. Based on these relationships for the pressure coefficient, Davis developed a predictor-corrector method which designs to a target pressure distribution. Surface corrections are determined by one of two design algorithms which utilize the wavy-wall relationships for the pressure coefficient. The choice of design algorithm depends on whether the local Mach number is less than or greater than unity. The two additional terms added to the McFadden algorithm (ref. 13) are the nondimensional time derivatives of the airfoil slope and curvature, and both terms are used regardless of the local Mach number. The modified method appears as

$$\beta_0 \frac{\partial (z_s/c)}{\partial t} + \beta_1 \frac{\partial^2 (z_s/c)}{\partial x \, \partial t} + \beta_2 \frac{\partial^3 (z_s/c)}{\partial x \, \partial x \, \partial t} = q^2_{\text{target}} - q^2_{\text{calculated}} \tag{7}$$

Using finite-difference techniques and allowing Δt to be unity (i.e., one design step), we may write the design algorithm for the jth point as

$$\beta_0 \Delta (z_s/c)_j + \beta_1 \frac{\Delta (z_s/c)_j - \Delta (z_s/c)_{j-1}}{\Delta x} + \beta_2 \frac{\Delta (z_s/c)_{j-1} - 2\Delta (z_s/c)_j + \Delta (z_s/c)_{j+1}}{\Delta x^2} = \left(q^2_{\text{target}} - q^2_{\text{calculated}}\right)_j \tag{8}$$

Through combination of the $\Delta (z_s/c)$ terms, the algorithm becomes

$$\Delta (z_s/c)_{j+1} \left(\frac{\beta_2}{\Delta x^2}\right) + \Delta (z_s/c)_j \left(\beta_0 + \frac{\beta_1}{\Delta x} - \frac{2\beta_2}{\Delta x^2}\right) + \Delta (z_s/c)_{j-1} \left(-\frac{\beta_1}{\Delta x} + \frac{\beta_2}{\Delta x^2}\right) = \left(q^2_{\text{target}} - q^2_{\text{calculated}}\right)_j \tag{9}$$

This equation is diagonally dominant and therefore may be solved through the use of a tridiagonal method. The coefficients β_0, β_1, and β_2 were determined by numerical experimentation to be 0.16, 1.00, and 0.50, respectively (ref. 17). These values were used initially for all design cases. These coefficients are discussed in more detail subsequently in this paper.

The design procedure is initiated after an initial solution for the starting geometry has been obtained. Target pressures are input to begin the design procedure. All modifications are applied to wing sections at the input span stations rather than at the computational span stations. If a target pressure distribution is desired at a span station that does not correspond to an input station, a new user-defined wing section is generated at that span location through interpolation.

As stated previously, modifications to the wing (or airfoil) sections consist of increments to the geometry normal to the wing plane. These incremental changes are applied to user-defined wing sections at each computational wing fine-grid point in the x-direction; that is, incremental changes are applied at every 1-percent-chord point downstream of the leading edge. The leading-edge and trailing-edge points

of the wing sections are held fixed since their surface velocities cannot be accurately computed by this analysis code. Boundary conditions are then recalculated for the modified wing geometry. Several analysis iterations, usually 10, are performed on the modified geometry and the pressures are again compared with the target pressures. This cycle of comparing pressure coefficients and modifying the geometry is referred to as a design step. The number of design steps needed to reach the target pressure distribution varies according to the severity of the changes required to the initial wing (or airfoil) geometry. This is not to say that the target pressure distribution is reached for every design case. There are many situations in which the design cannot be obtained, such as specification of an unrealistic target pressure distribution or too severe a change between the target and initial pressure distributions. At this time no test is used to determine if the designed pressure distribution is reasonably close to the target pressure distribution. Instead, the user specifies the number of design steps to be taken.

The design code is set up to redesign the upper surface and the lower surface independently, so single-surface design (holding the other surface fixed) is an option. Since all modifications are made to the actual geometry, the geometric modifications can easily be constrained by the user if desired.

Design Test Cases

Several design test cases were considered to verify the compatibility of the design algorithm and the analysis code and to demonstrate the capabilities of the design algorithm. Two-dimensional cases were initially considered, the first being a subcritical target pressure distribution and the second a test case where there is a significant region of supercritical flow and a well-defined shock. A three-dimensional test case then followed for a swept and tapered planform. Also, two previous design efforts with a cut-and-try approach were repeated utilizing the automated computational design code. For the test cases presented, aerodynamic calculations were made on the final design geometry and the resulting pressure distribution was compared with the target pressure distribution.

The first two design test cases were two-dimensional and used an NACA 0006 airfoil as the starting geometry. The target pressure distribution for both cases was that of an NACA 0012 airfoil at the particular flow conditions. The first case was executed at a free-stream Mach number of $M_\infty = 0.70$ and $\alpha = 1.0°$. This case required 30 design steps to approximate the target pressure distribution. (See fig. 5(a).) Comparisons of the design airfoil ordinates with the NACA 0012 ordinates yielded root-mean-square (rms) errors of 0.00262 for the upper surface and 0.00215 for the lower surface. The rms error was much larger than might be expected considering the good agreement of the design and target pressures shown in figure 5(a). As shown in figure 5(b), the differences in the surface ordinates appear to have been the result of an angle-of-attack change. However, the leading-edge point ($x/c = 0$) and the trailing-edge point ($x/c = 1.0$) were held fixed during the design process and angle of attack was not allowed to change. It was then conjectured that the camber line of the design airfoil differed from that of the NACA 0012, which could simulate the target airfoil at a lower angle of attack. In figure 6 the camber lines of the design and target airfoils are shown. As is shown in the figure, the camber line of the design airfoil was below that of the NACA 0012. The design airfoil was then rotated about the trailing edge 0.15°, based on the angle of the camber line of the design airfoil, and compared with the NACA 0012 airfoil (fig. 7). The rms error was reduced to 0.00134 on the upper surface and 0.00123 on the lower surface. Aerodynamic calculations were made for the NACA 0012 at $M_\infty = 0.70$ and $\alpha = 1.0°$ and 0.85°; these calculations showed no discernible changes in the pressure distribution. Based on the information obtained through rotation of the design airfoil and by assessment of the effects of small angle-of-attack changes on the pressure distribution of the NACA 0012, the design geometry obtained for this design test case was reasonable. This design case illustrated a certain lack of sensitivity of the target pressure distribution to small changes in the design geometry.

The next case, at $M_\infty = 0.80$ and $\alpha = 0°$, was a more difficult design problem in that there is a significant difference in the extent of supersonic flow over the NACA 0012 and the NACA 0006 airfoil at $M_\infty = 0.80$. Fifty design steps were needed to match the target pressure distribution (fig. 8(a)). A comparison of the design and NACA 0012 airfoils is shown in figure 8(b). The rms error between the design and the NACA 0012 airfoil was 0.00163 for the upper and lower surfaces. Oscillations which occurred in the pressure distribution at the base of the shock were eliminated after an additional 140 aerodynamic calculations on the final design geometry (fig. 9).

Upon completion of these two-dimensional design test cases, a three-dimensional design test case was performed. For this case, a swept, tapered planform was used for the starting geometry, with the entire wing made up of NACA 0006 airfoils (fig. 10). The planform had 20° of leading-edge sweep, an aspect

ratio of 7.2, and a taper ratio of 0.26. Only airfoil sections at two locations were used to define the wing, one at the root and one at the tip. The design task was to modify the wing section at $\eta = 0.665$ so that the pressure distribution for the NACA 0012 airfoil at the design conditions would be obtained at this wing station.

This was a difficult design test case because at $M_\infty = 0.90$ and $\alpha = 0°$ a strong shock occurred in the target pressure distribution at $\eta = 0.665$, where the NACA 0012 airfoil was located (fig. 11). Figure 11 shows the design and target pressure coefficients after 40 design steps for $\eta = 0.665$ and for several other span stations. Oscillations about the shock were caused by irregularities in the surface slopes and curvature in that region. The pressure distributions at span stations other than $\eta = 0.665$, although labeled as target pressures, were actually known pressures for the desired configuration. As described above, the desired configuration had the same planform as the initial geometry with NACA 0006 sections defining the root and the tip and with an NACA 0012 airfoil at $\eta = 0.665$. Only the airfoil at $\eta = 0.665$ was changed with the design algorithm. Computational airfoils inboard and outboard of $\eta = 0.665$ were determined through spanwise interpolation, which accounts for the oscillations in the pressure distributions at span stations other than the design station. A comparison of the design airfoil ordinates with the NACA 0012 airfoil ordinates (fig. 12) resulted in an rms error of 0.001191 for the upper and lower surfaces. The design airfoil ordinates were smoothed with a least-squares fit to a cubic polynomial with a square root term added in the leading-edge region. The smoothed ordinates were substituted for the initial NACA 0006 ordinates at $\eta = 0.665$ and an analysis run was subsequently made on this new wing geometry. Results from the analysis run compared well with the desired target pressures and are illustrated in figure 13.

Also considered were two additional test cases based on actual designs previously completed by means other than automated computational design. One was originally addressed by Campbell, Waggoner, and Phillips (ref. 4), who relied on computational analyses during the design of a natural laminar flow (NLF) airfoil at transonic conditions. The design approach was based on the cut-and-try method with an airfoil analysis code. The starting point for this design was a modified 14-percent-thick NLF airfoil developed by Viken (ref. 24). Viken's original airfoil was modified to lower the design lift coefficient by reducing the trailing-edge camber. Analysis of the initial geometry at $M_\infty = 0.70$ and $\alpha = -0.193°$ revealed two undesirable features in the pressure distribution of this airfoil (fig. 14) that were eliminated using the cut-and-try design approach. The pressure peak at the leading edge of the lower surface was undesirable since it could cause transition of the boundary layer. The second undesirable feature was the steep pressure recovery region on the upper surface, which could cause the flow to separate. The expansion ahead of the shock was not present in the results from the full-potential methods used in reference 3. The final-design airfoil of Campbell et al. is designated the HSNLF-0213. Figure 15 illustrates the initial pressure distribution, the target pressure distribution (of the final airfoil of ref. 4), and the design pressure distribution after 40 design steps using the current design code. Although the target and design pressure coefficients were reasonably matched, there is a significant difference between the design airfoil and the HSNLF-0213 airfoil. One factor that may have contributed to the discrepancies in this design case is a possible path dependency of the design algorithm. This was the only design test case attempted where the initial geometry was thicker than the desired final geometry. In order to investigate this possible problem, another design case based on the HSNLF-0213 airfoil but with a flat plate as the initial geometry was then attempted. The results after 30 design steps (fig. 16) showed that the design pressures again matched the target pressures very well, but the agreement between the design airfoil and the HSNLF-0213 airfoil was much improved. These results indicate that the direction of change to the airfoil surface might be critical in the design process.

The second design case attempting to duplicate a previous design task was based on modifications made by hand to the root of a supercritical wing as part of a research study on supercritical wings (ref. 25). The wing planform selected for modification had 30° of sweep at the quarter-chord of the outer portion of the wing and an aspect ratio of 9.8. A leading-edge extension was added at the root to increase structural depth (fig. 17). The coordinates for the final wing geometry were available and used to generate target pressure distributions for wing sections inboard of the break. The initial geometry for the inboard sections could not be located, so the NACA 0006 airfoil was used as the starting geometry in the region to be designed. The fuselage was modeled by an axisymmetric body with a maximum radius of 11.7 in. Figure 18 illustrates the target and design pressure distributions at $M_\infty = 0.83$ and $\alpha = 2.19°$ for several span stations after 40 design cycles. Oscillations occurred in the pressure distributions at all design span stations. Based on the third design test case, the design airfoils were smoothed

and used as the starting geometry for a second design run. After 30 additional design steps the results had improved, but oscillations were still present at the more outboard stations. The design airfoils were again smoothed and used as the starting geometry for a third design run. Figure 19 shows the results after 30 additional design steps. Good agreement with the target pressure coefficients was obtained at the inboard stations, but as the shock strength increased outboard so did the oscillations in the pressure coefficients at the shock. Comparisons of four of the design airfoils with the actual airfoils used to generate the target pressures are shown in figure 20. Excellent agreement is shown for the lower surface, even in the cove region. Differences in the upper surfaces vary with each span station, with the largest discrepancy occurring at the most outboard station. This was the most difficult design test case attempted. Supercritical airfoils such as those desired in the inboard region are very sensitive to small changes in the flow conditions, and this sensitivity, as shown in previous design cases, complicates the design task. The algorithm did, however, modify the wing sections in such a way as to result in a wing geometry much closer to that desired than to the initial wing geometry.

Design Code Coefficient Selection

The design algorithm used by the subject code contains three coefficients, β_0, β_1, and β_2, for which the values can be changed by the user. The default values have been determined by numerical experimentation to be 0.16, 1.00, and 0.50 for β_0, β_1, and β_2, respectively (ref. 17). These values, however, were not believed to be the optimum values for all design cases. A series of design computations were performed to study the effects of the values of β_0, β_1, and β_2 on the design process and to determine how these values should be selected for a particular design problem. The values of β_0, β_1, and β_2 were chosen such that all either increased or decreased by the same factor over the default values. It was also found during this series of design computations that the value of the subsonic relaxation factor ω, which is used by the analysis code to accelerate the flow solution, also has an effect on the design results. Preliminary guidelines based on these design runs for using the design code were determined to be as follows:

1. For design test cases where both the initial and final pressure distributions are subcritical, use $\beta_0 = 0.16$, $\beta_1 = 1.00$, $\beta_2 = 1.00$, and $\omega = 1.5$.
2. For design test cases where there is a significant difference in the amount of supersonic flow between the initial and final pressure distributions, use $\beta_0 = 0.32$, $\beta_1 = 2.00$, $\beta_2 = 1.00$, and $\omega = 1.8$.

All design cases presented in this paper utilized the above guidelines.

Upon completion of the initial design test cases, additional design cases were run for which the values of the design coefficients were allowed to change relative to one another. Several of these design computations were performed with two of the three design coefficients equal to zero. The third coefficient varied for each design run to determine its individual effect on the design. In addition, design computations were performed for which the values of the design coefficients were determined by the previously discussed preliminary guidelines, with the exception of one coefficient. For this particular coefficient, a set of design computations was made in which the value of this coefficient increased and decreased from the preliminary guideline value. This procedure was followed for all three design coefficients. All design computations were made at both supersonic and subsonic conditions with the NACA 0006 airfoil as the initial geometry and the target pressure distribution of the NACA 0012 airfoil at the design conditions.

The results of the above design computations showed that the coefficient β_1 was more influential than the other two coefficients when the flow field was primarily supersonic. Also demonstrated was the stronger influence of the β_2 coefficient for subsonic flow. The coefficient β_0 had virtually no effect on the design for both supersonic and subsonic conditions. These results are in accordance with those obtained by Davis (ref. 22) and Campbell and Smith (ref. 26), each of whom developed similar design algorithms.

Concluding Remarks

A three-dimensional transonic design code has been developed that predicts wing contour modifications to achieve a specified pressure distribution. The analysis portion of the design code is a transonic-small-disturbance code applied to the wing, body, pods, pylons, and winglet. This analysis code has been used extensively on a wide variety of configurations, a fact which lends confidence to the results obtained when coupled with a design algorithm. An additional benefit of using this code is its capability for two-dimensional analysis, which means two-dimensional design is an option. The design algorithm employed relates changes in surface velocities to changes in the geometry.

Several two- and three-dimensional design test cases were considered to demonstrate the capabilities of the design code. The design cases were generally

successful, the exception being a three-dimensional supercritical-wing design case. The results of the design test cases have led to the following conclusions and recommendations concerning the design code:

1. The design code developed during this study is operational, as demonstrated by various two- and three-dimensional test cases.

2. Based on initial studies, two sets of values for the design coefficients β_0, β_1, and β_2 and for the subsonic relaxation factor have been determined. One set of values is for supersonic target pressure distributions and the other is for subsonic target pressure distributions.

3. Based on a series of design runs made after the completion of the design test cases, it was found that for supersonic flow the design coefficient β_1 was more influential than β_0 or β_2 on the design. For subsonic flow, β_2 was the most influential. The coefficient β_0 had virtually no effect on the design at either supersonic or subsonic conditions.

4. Although the target pressure coefficients are achieved, additional design steps may be necessary because of the lack of sensitivity of the final wing (or airfoil) shape to small changes in the flow conditions.

5. Further studies need to be conducted on the effects of starting with a wing (or airfoil) that is thicker than the final-design wing (or airfoil).

6. In order to glean the full benefits of the design algorithm, a systematic study to determine the optimum values for β_0, β_1, and β_2 for various flow conditions needs to be conducted.

NASA Langley Research Center
Hampton, Virginia 23665-5225
February 5, 1988

References

1. Boppe, Charles W.: *Transonic Flow Field Analysis for Wing-Fuselage Configurations.* NASA CR-3243, 1980.
2. Boppe, Charles W.: *Aerodynamic Analysis for Aircraft With Nacelles, Pylons, and Winglets at Transonic Speeds.* NASA CR-4066, 1987.
3. Waggoner, Edgar G.; Campbell, Richard L.; and Phillips, Pamela S.: Computational Wing Design in Support of an NLF Variable Sweep Transition Flight Experiment. AIAA-85-4074, Oct. 1985.
4. Campbell, Richard L.; Waggoner, Edgar G.; and Phillips, Pamela S.: Design of a Natural Laminar Flow Wing for a Transonic Corporate Transport. AIAA-86-0314, Jan. 1986.
5. Hicks, Raymond M.; and Henne, Preston A.: Wing Design by Numerical Optimization. AIAA-77-1247, Aug. 1977.
6. Aidala, P.: *Numerical Aircraft Design Using 3-D Transonic Analysis With Optimization. Volume III, Part 2: User's Guide to Fighter Design Computer Program.* AFWAL-TR-81-3091, Vol. III, Pt. 2, U.S. Air Force, Aug. 1981. (Available from DTIC as AD A110 037.)
7. Davis, Warren H., Jr.; Aidala, Paul V.; and Mason, William H.: *A Study To Develop Improved Methods for the Design of Transonic Fighter Wings by the Use of Numerical Optimization.* NASA CR-3995, 1986.
8. Fung, K.-Y.; Sobieczky, H.; and Seebass, R.: Shock-Free Wing Design. *AIAA J.*, vol. 18, no. 10, Oct. 1980, pp. 1153–1158.
9. Yu, N. J.: Efficient Transonic Shock-Free Wing Redesign Procedure Using a Fictitious Gas Method. *AIAA J.*, vol. 18, no. 2, Feb. 1980, pp. 143–148.
10. Shankar, V.: A Full Potential Inverse Method Based on a Density Linearization Scheme for Wing Design. AIAA-81-1234, June 1981.
11. Henne, P. A.: Inverse Transonic Wing Design Method. *J. Aircr.*, vol. 18, no. 2, Feb. 1981, pp. 121–127.
12. Tranen, T. L.: A Rapid Computer Aided Transonic Airfoil Design Method. AIAA Paper No. 74-501, June 1974.
13. Garabedian, Paul; and McFadden, Geoffrey: Design of Supercritical Swept Wings. *AIAA J.*, vol. 20, no. 3, Mar. 1982, pp. 289–291.
14. Takanashi, S.: Iterative Three-Dimensional Transonic Wing Design Using Integral Equations. *J. Aircr.*, vol. 22, no. 8, Aug. 1985, pp. 655–660.
15. Carlson, Leland A.: *Transonic Airfoil Design Using Cartesian Coordinates.* NASA CR-2578, 1976.
16. Raj, Pradeep: Shockfree Advanced Supercritical Wing Design. LR-29697, Lockheed-California Co., May 15, 1981.
17. Raj, Pradeep; and Reaser, J. S.: *An Improved Full-Potential Finite-Difference Transonic-Flow Code (FLO 22.5) for Wing Analysis and Design.* LR 29759, Lockheed-California Co., Nov. 1981.
18. Burris, C. B.; Haney, H. P.; and Sankar, N. N.: Computational Aerodynamic Design Methodology. AIAA-83-1865, July 1983.
19. Barger, Raymond L.; and Brooks, Cuyler W., Jr.: *A Streamline Curvature Method for Design of Supercritical and Subcritical Airfoils.* NASA TN D-7770, 1974.
20. Shankar, Vijaya; Malmuth, Norman D.; and Cole, Julian D.: Computational Transonic Design Procedure for Three-Dimensional Wings and Wing-Body Combinations. AIAA Paper 79-0344, Jan. 1979.
21. Vanderplaats, Garret N.: *CONMIN—A FORTRAN Program for Constrained Function Minimization, User's Manual.* NASA TM X-62282, 1973.
22. Davis, Warren H., Jr.: Technique for Developing Design Tools From the Analysis Methods of Computational Aerodynamics. AIAA Paper 79-1529, July 1979.
23. Liepmann, H. W.; and Roshko, A.: *Elements of Gasdynamics.* John Wiley & Sons, Inc., c.1957.
24. Viken, Jeffrey K.: *Aerodynamic Design Considerations and Theoretical Results for a High Reynolds Number Natural Laminar Flow Airfoil.* M.S. Thesis, George Washington Univ., Jan. 1983.

25. Bartlett, Dennis W.; and Patterson, James C., Jr.: *NASA Supercritical-Wing Technology.* NASA TM-78731, 1978.

26. Campbell, Richard L.; and Smith, Leigh A.: A Hybrid Algorithm for Transonic Airfoil and Wing Design. AIAA-87-2552-CP, Aug. 1987.

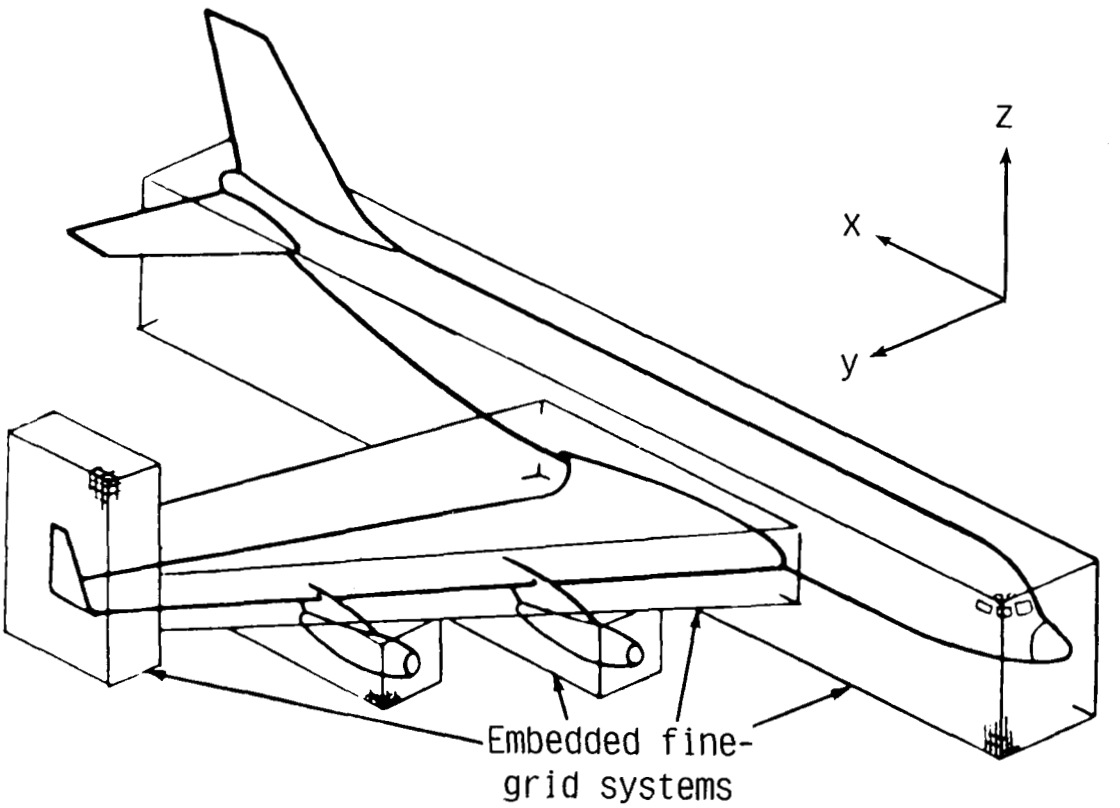

Figure 1. Computational fine-grid system. (From ref. 1.)

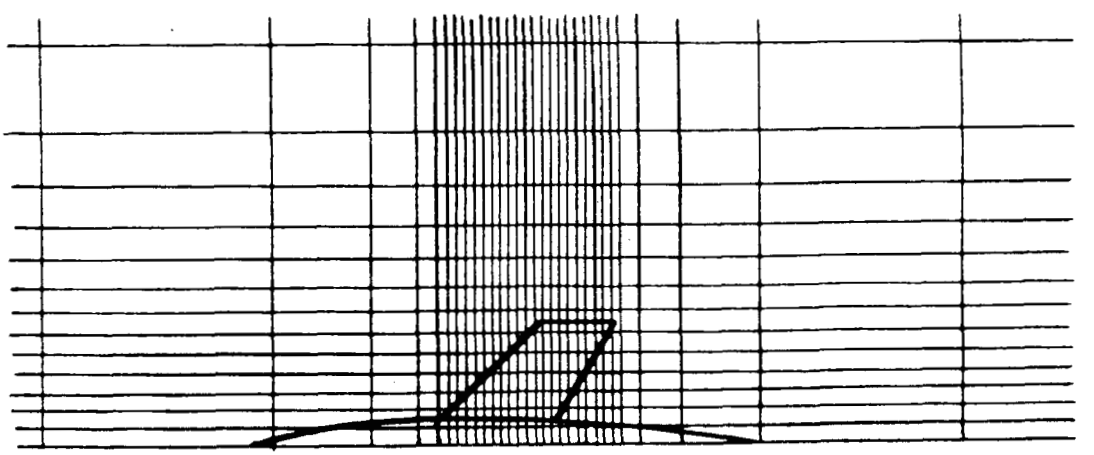

Figure 2. Crude grid stretching in x- and y-directions. (From ref. 1.)

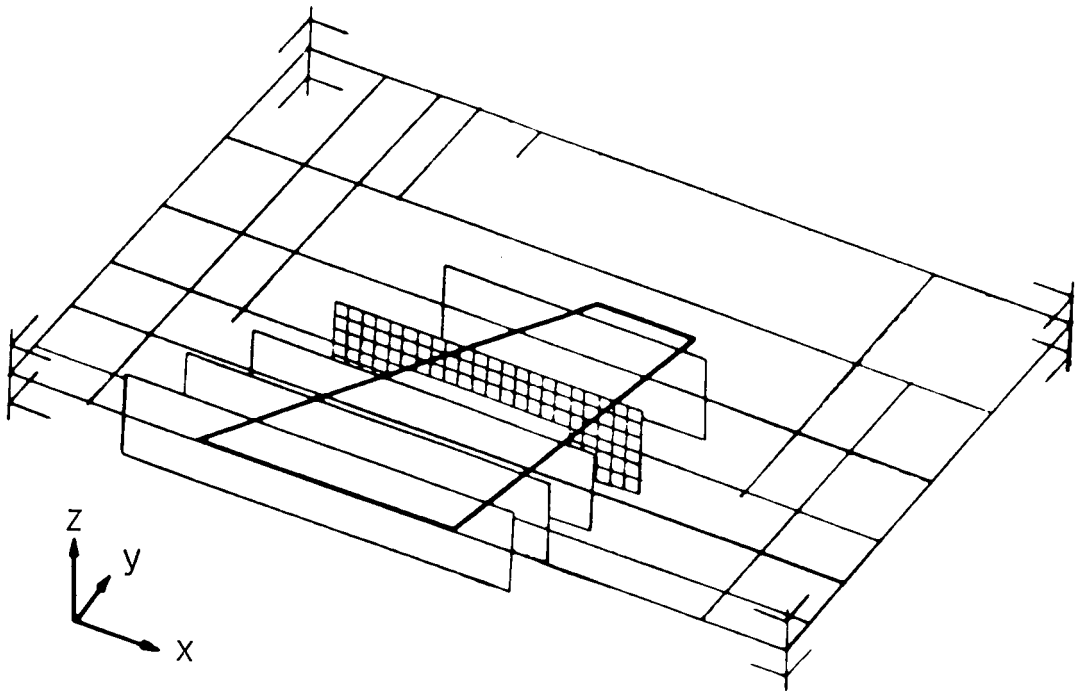

Figure 3. Wing fine-grid system. (From ref. 1.)

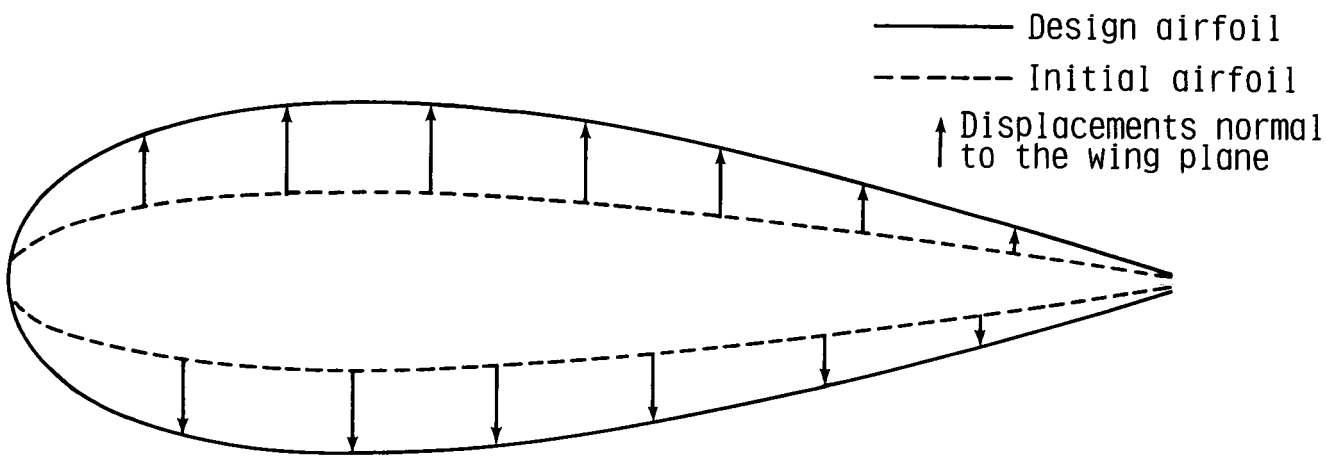

Figure 4. Contour changes to surface geometry.

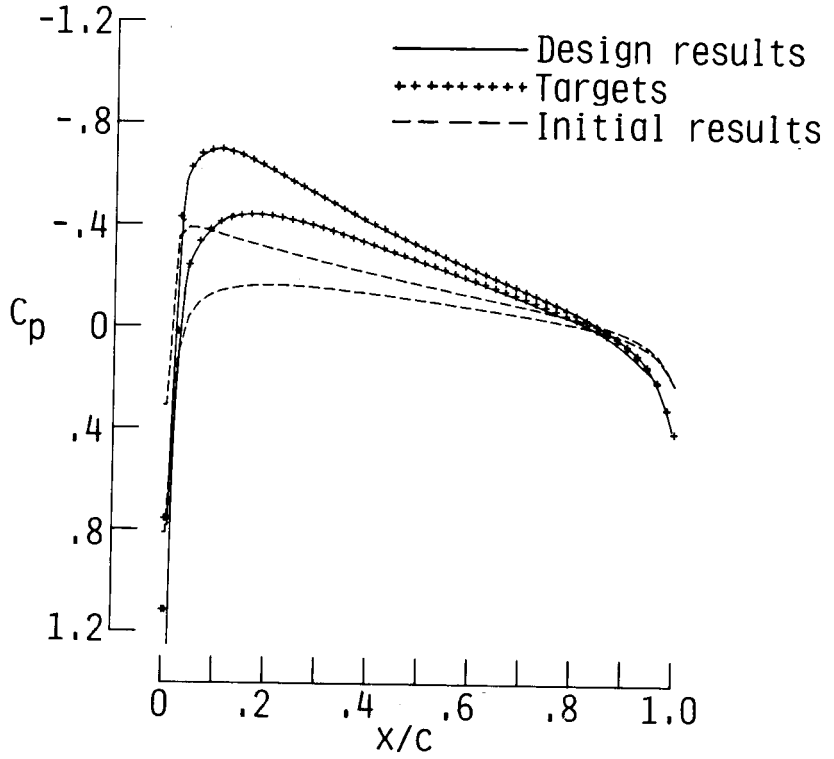

(a) Comparison of wing pressure distributions.

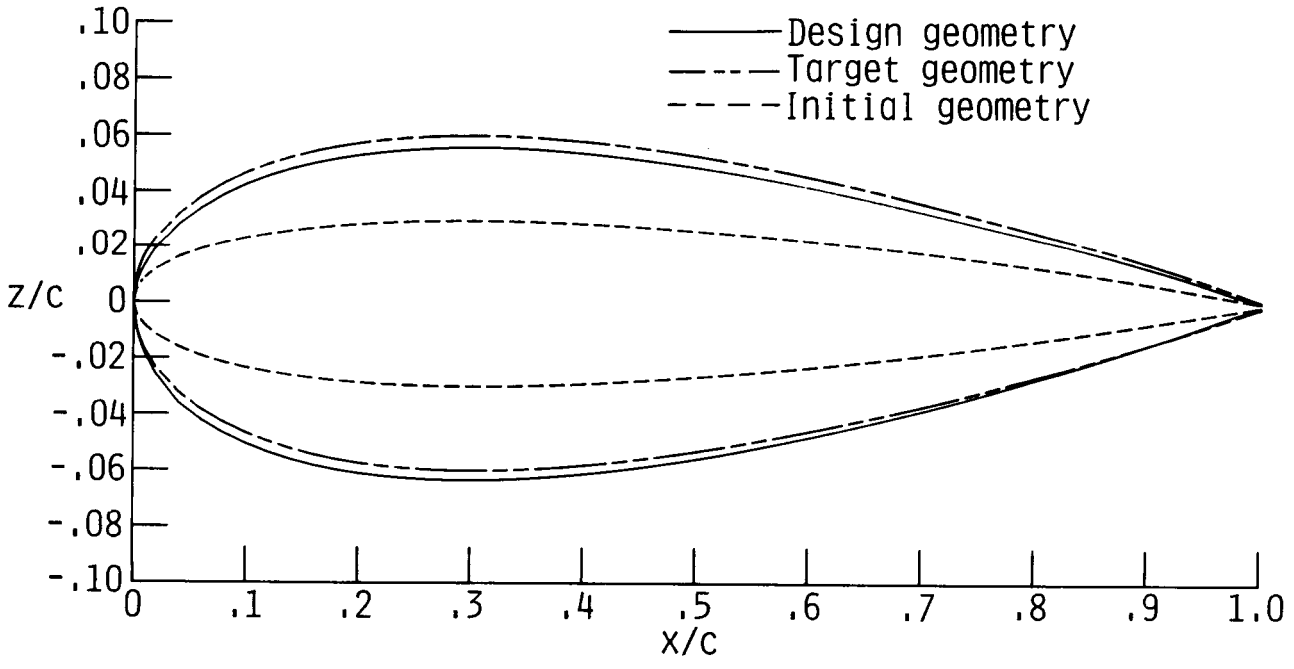

(b) Comparison of airfoil geometries.

Figure 5. Results for design test case with NACA 0006 airfoil as initial geometry and target pressure distribution of NACA 0012 airfoil at $M_\infty = 0.70$ and $\alpha = 1.0°$.

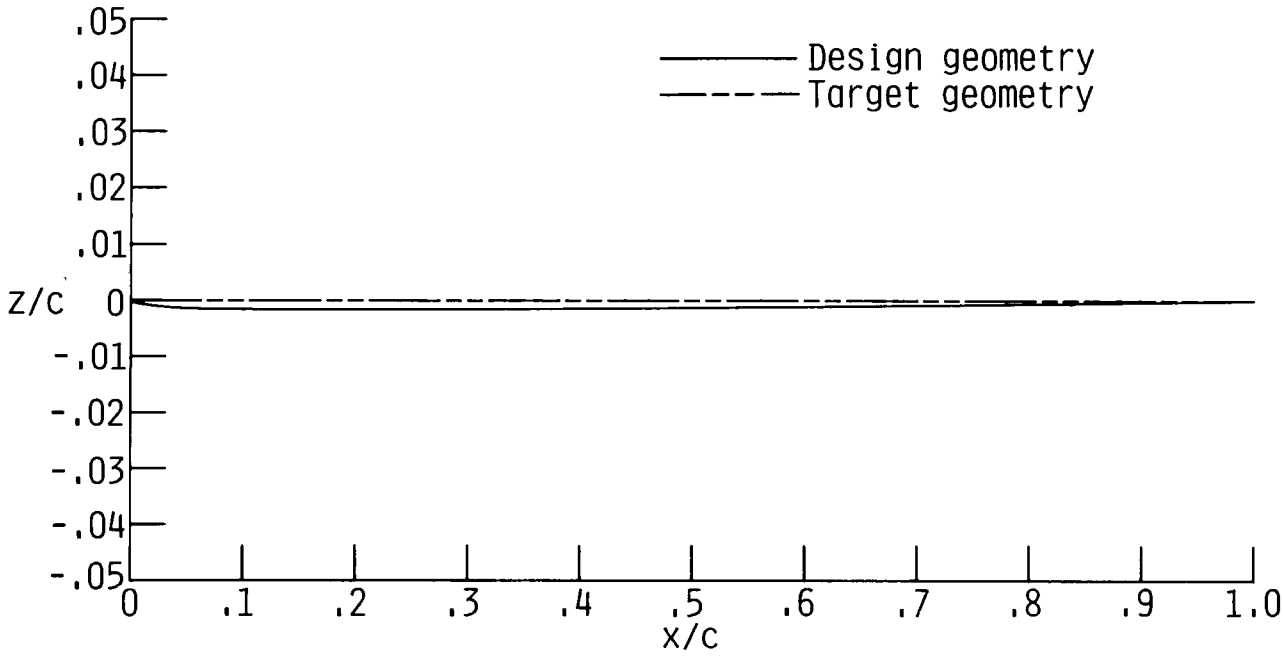

Figure 6. Camber lines of design airfoil and NACA 0012 (target) airfoil.

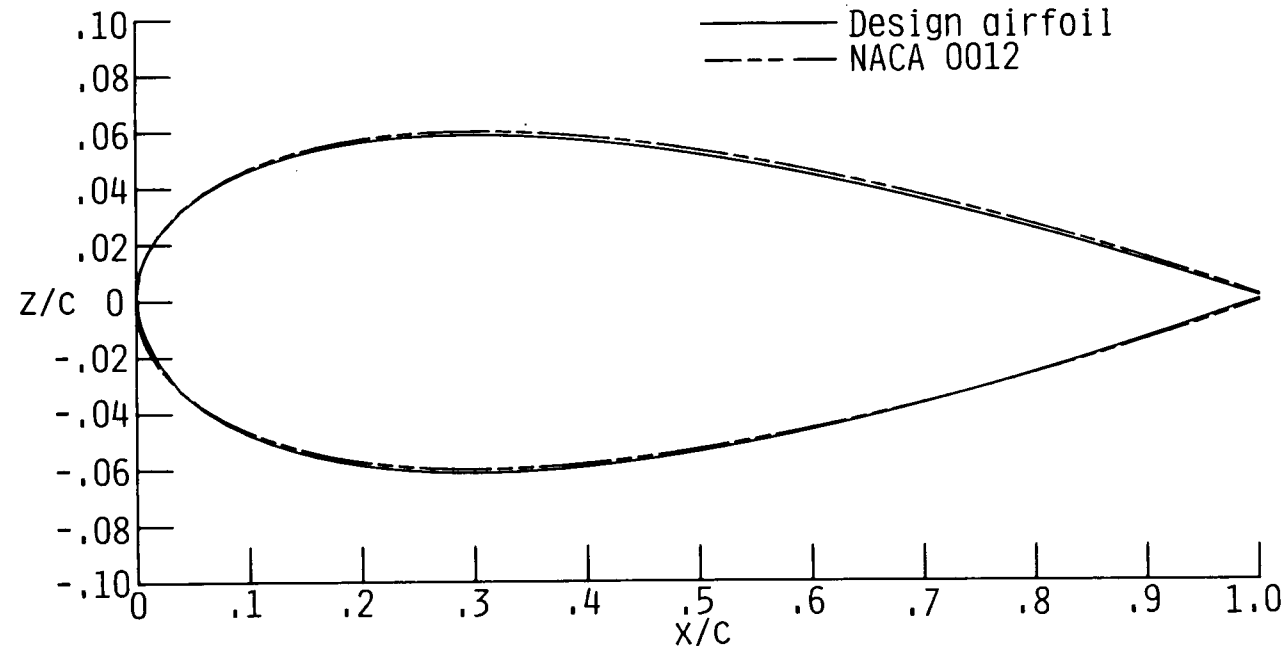

Figure 7. Comparison of design airfoil rotated 0.15° and NACA 0012 airfoil.

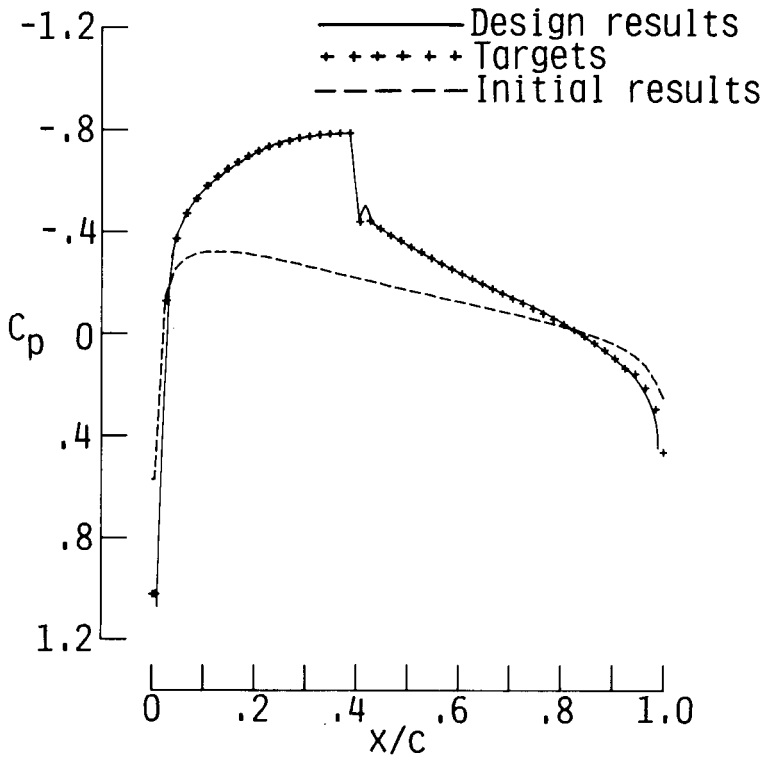

(a) Comparison of wing pressure distributions.

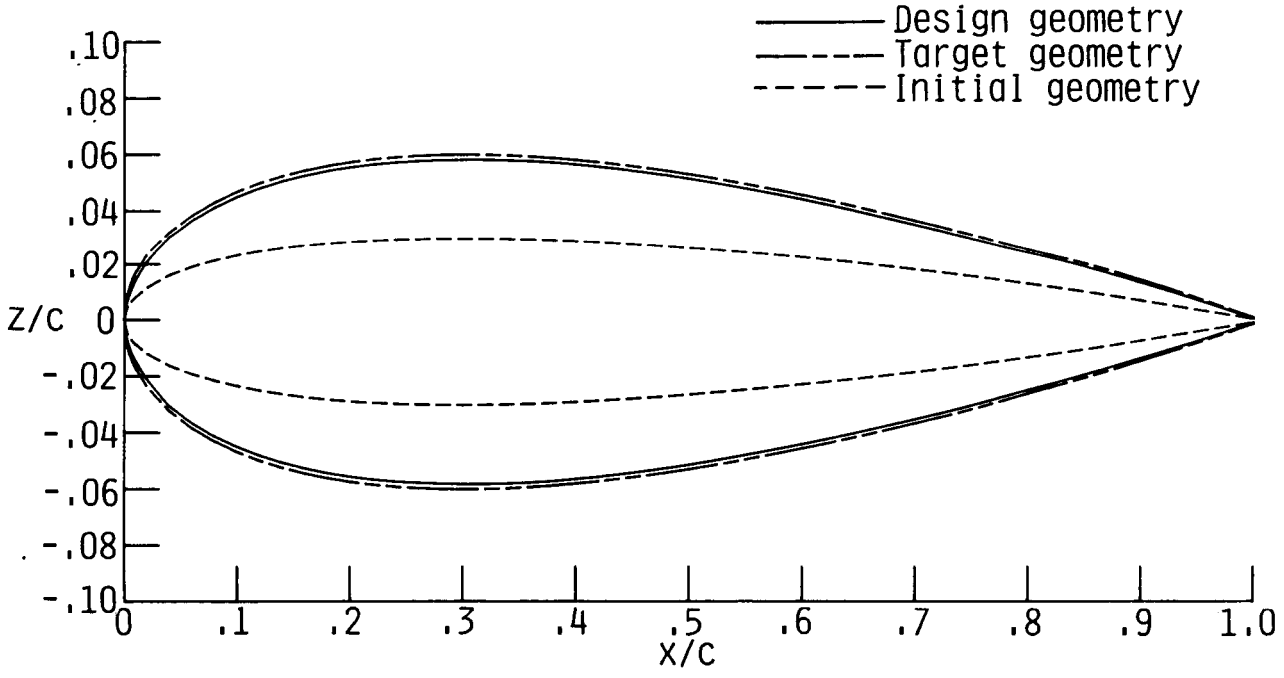

(b) Comparison of airfoil geometries.

Figure 8. Results for design test case with NACA 0006 airfoil as initial geometry and target pressure distribution of NACA 0012 at $M_\infty = 0.80$ and $\alpha = 0°$.

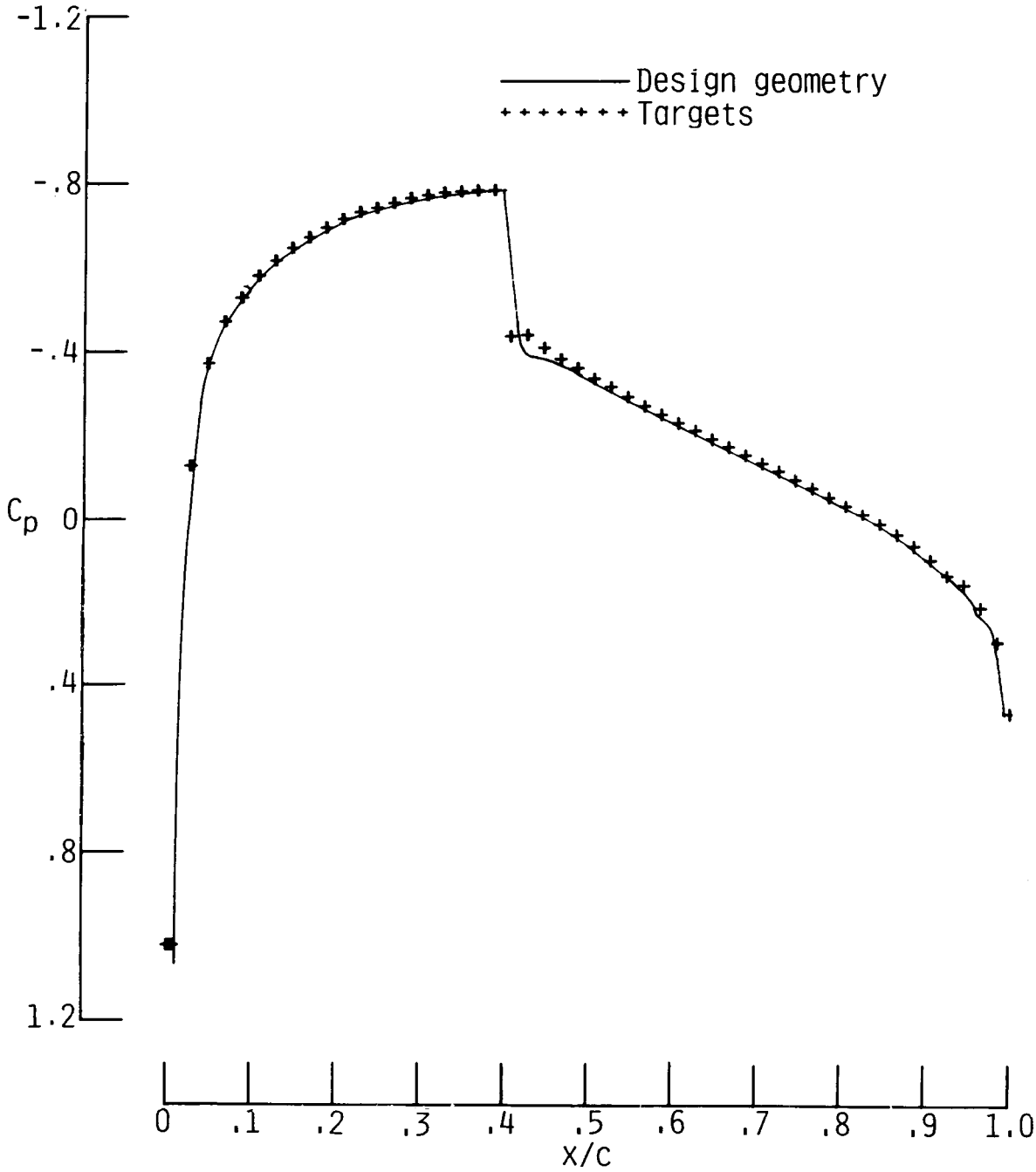

Figure 9. Pressure distribution for design geometry after additional iterations at $M_\infty = 0.80$ and $\alpha = 0°$.

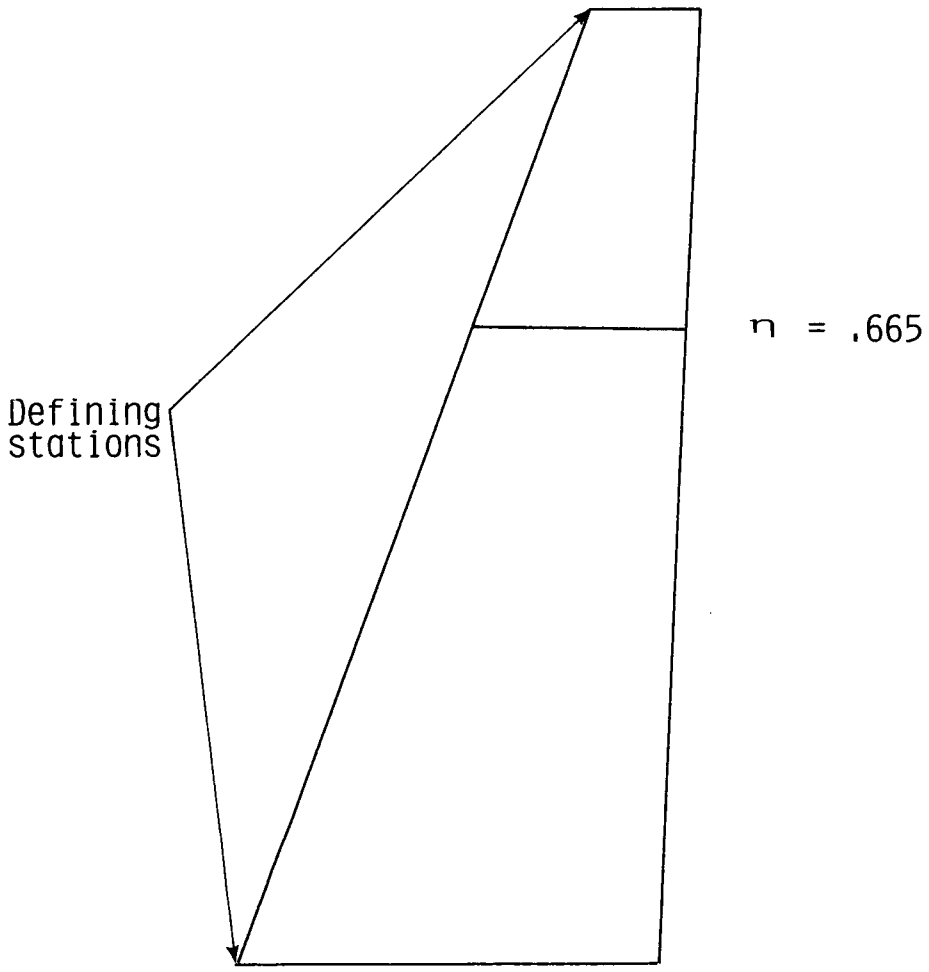

Figure 10. Planform definition for three-dimensional design test case at $M_\infty = 0.90$ and $\alpha = 0°$. Sweep = 20°; Aspect ratio = 7.2; Taper ratio = 0.26.

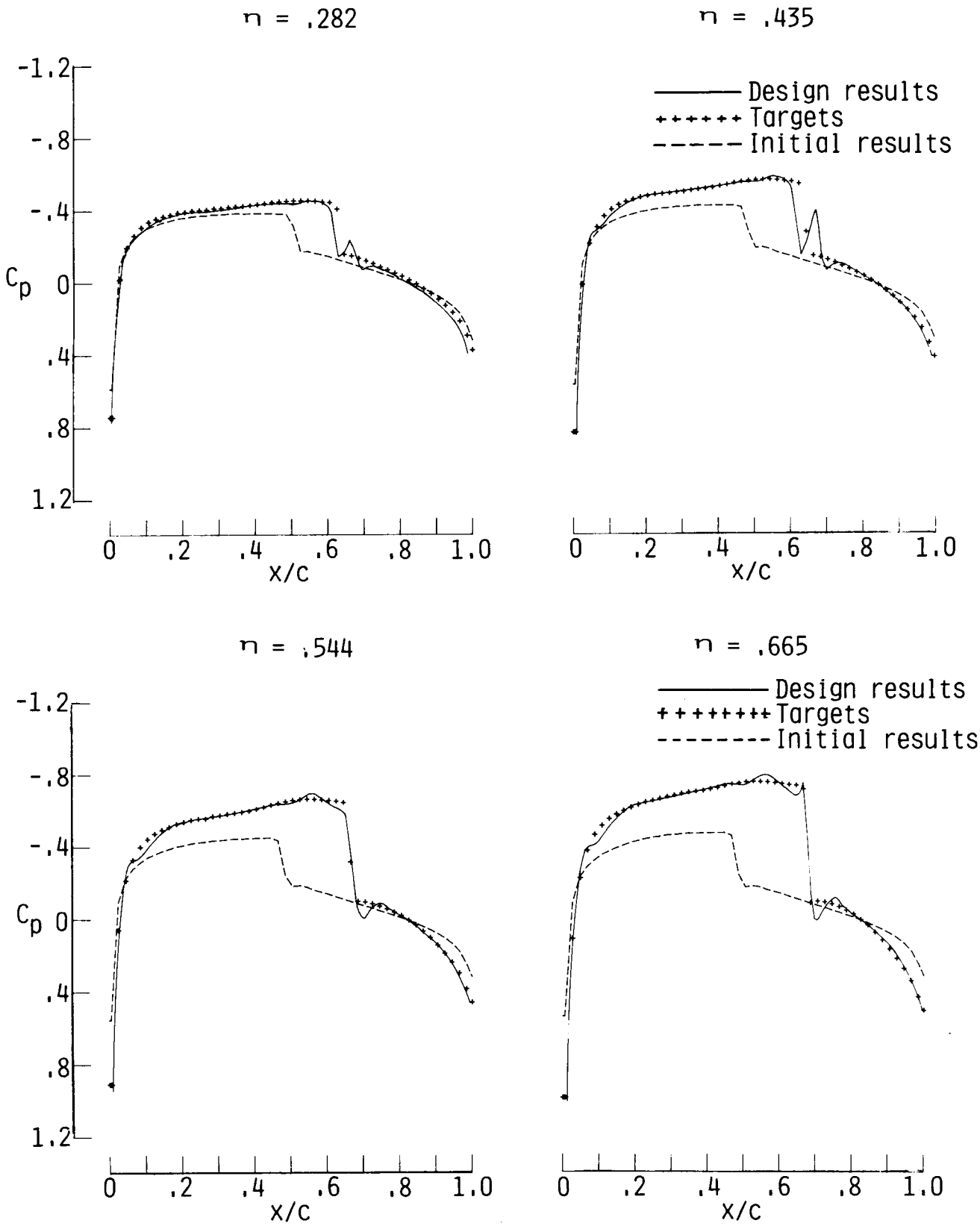

Figure 11. Results for design test case of swept, tapered wing with modified airfoil at $\eta = 0.665$ at $M_\infty = 0.90$ and $\alpha = 0°$.

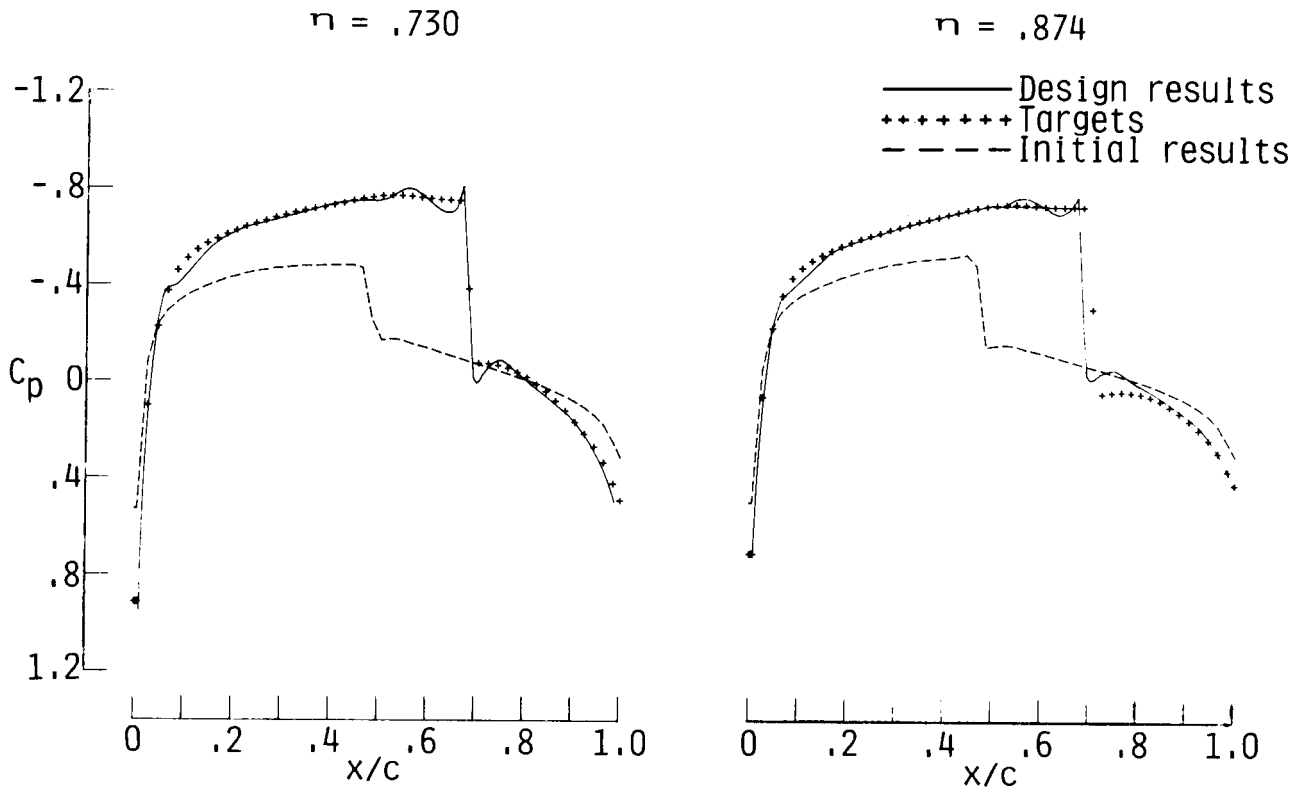

Figure 11. Concluded.

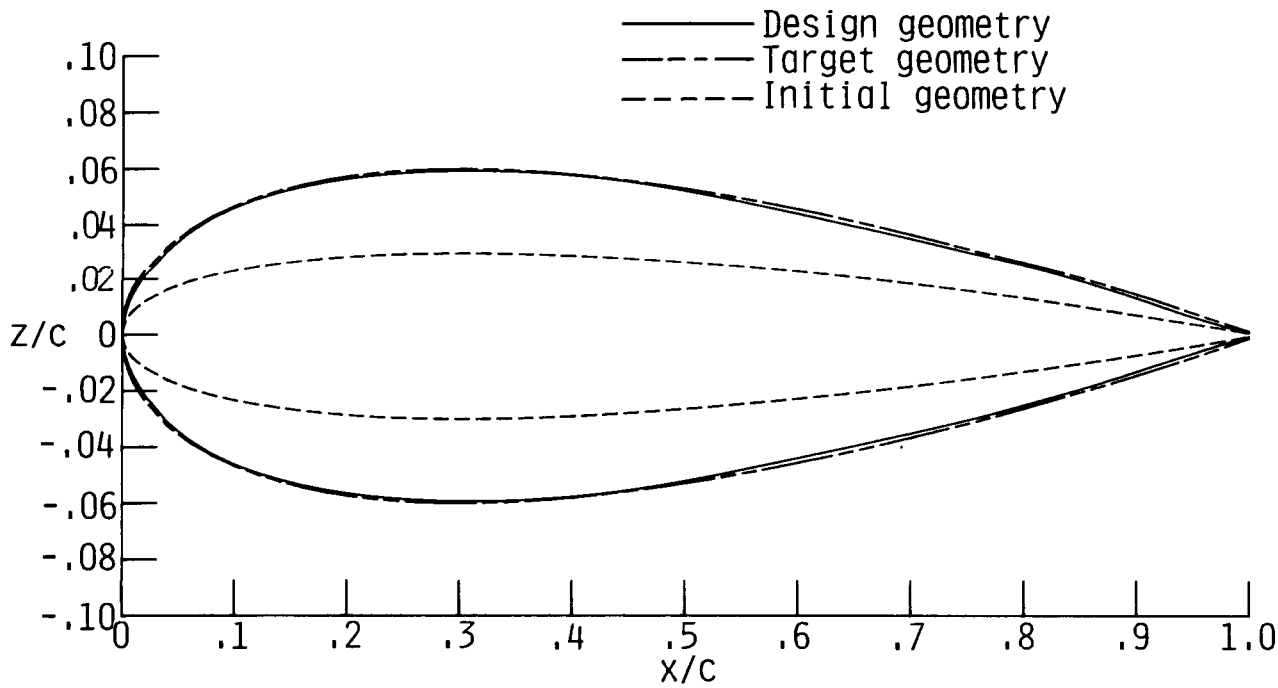

Figure 12. Comparison of design, target, and initial geometries.

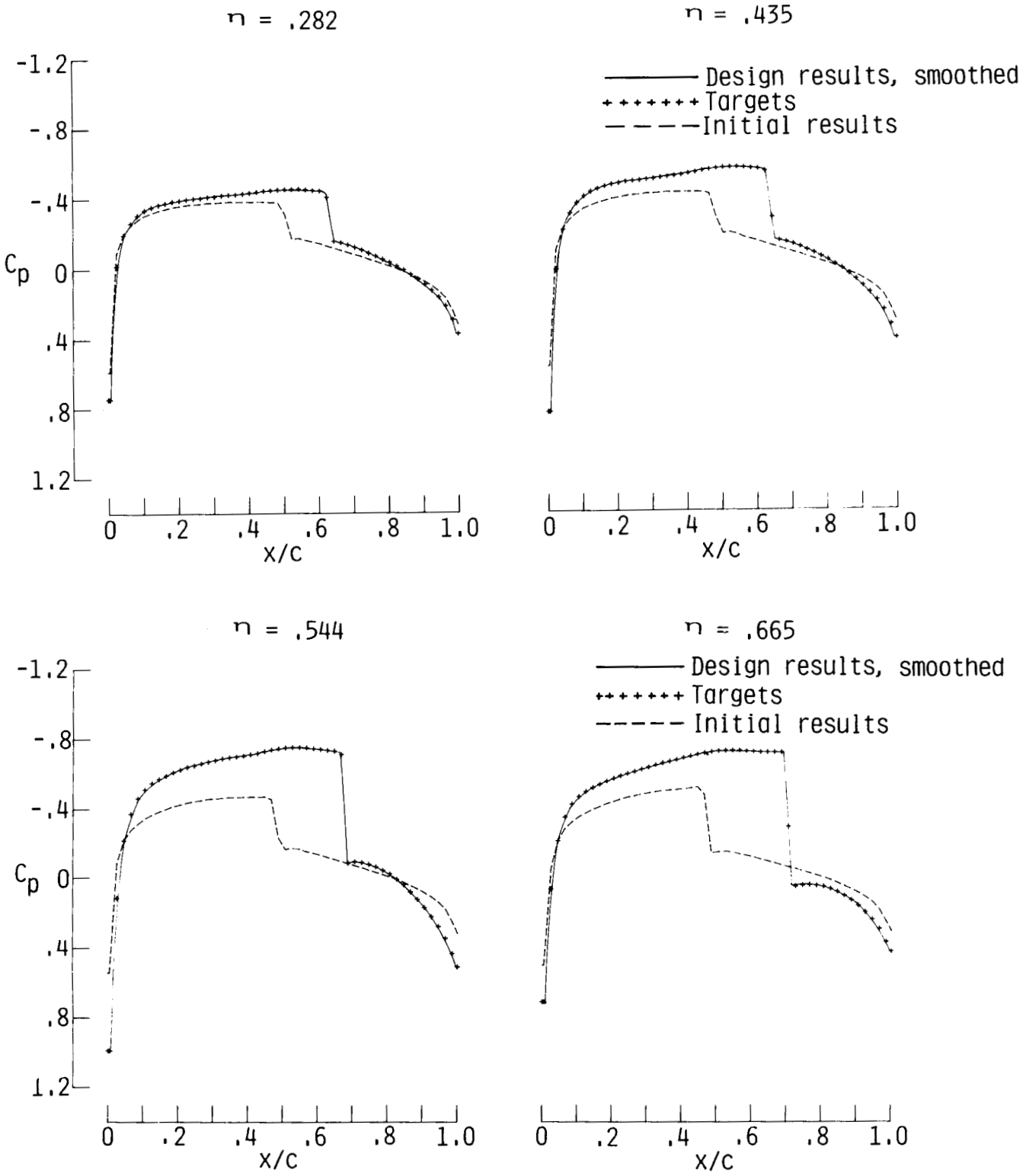

Figure 13. Results for new wing geometry with smoothed airfoil ordinates at $\eta = 0.665$ at $M_\infty = 0.90$ and $\alpha = 0°$.

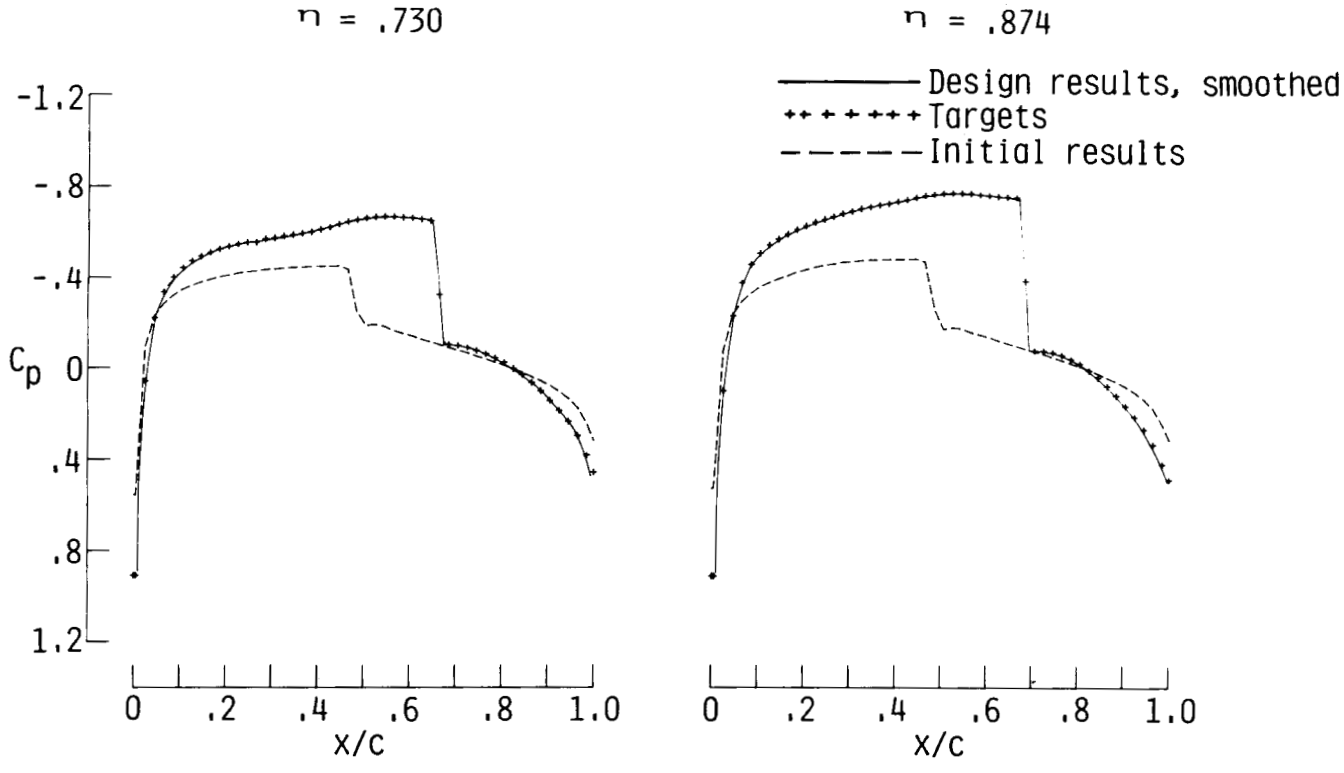

Figure 13. Concluded.

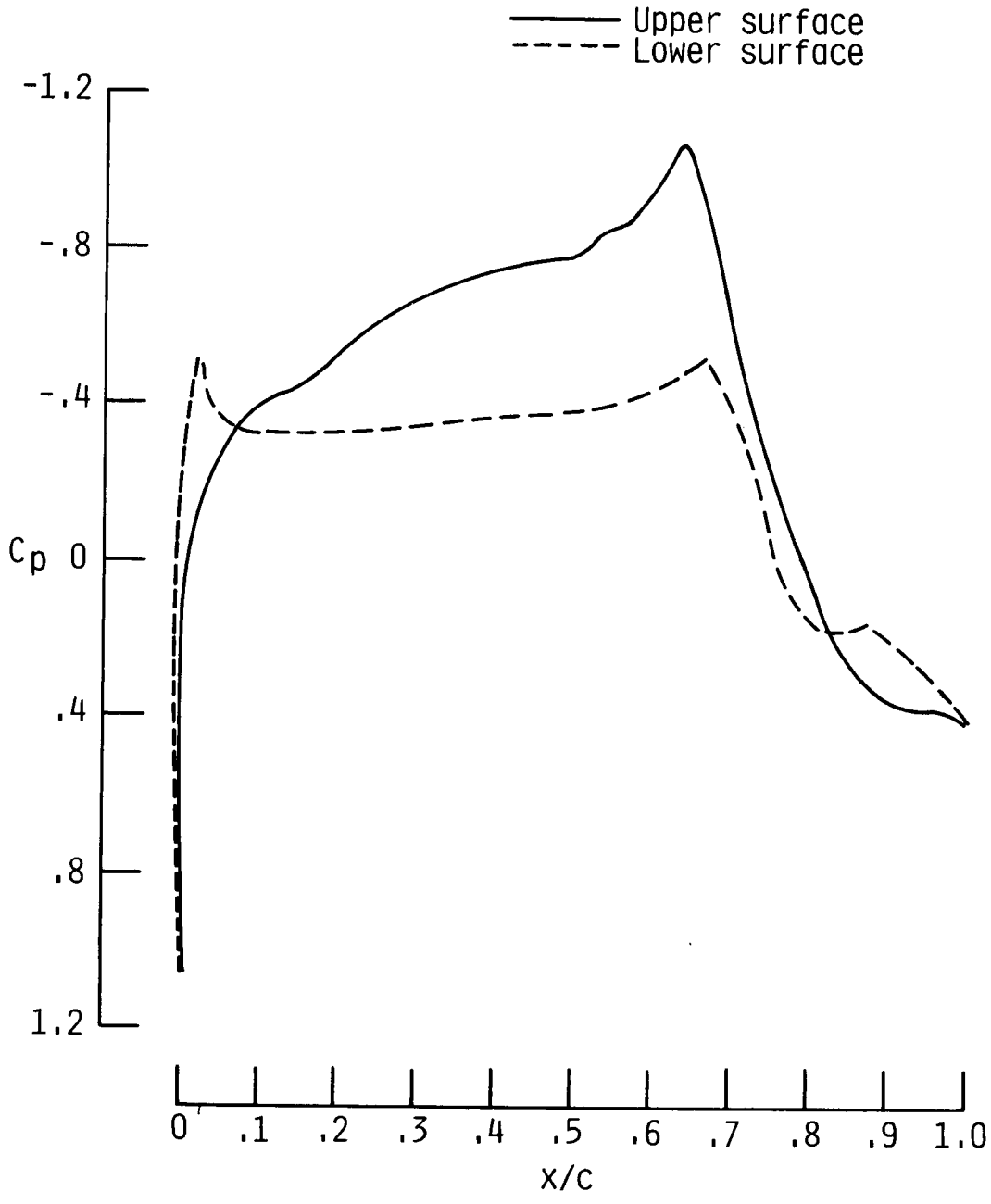

Figure 14. Pressure distribution for modified 14-percent-thick NLF airfoil at $M_\infty = 0.70$ and $\alpha = -0.193°$.

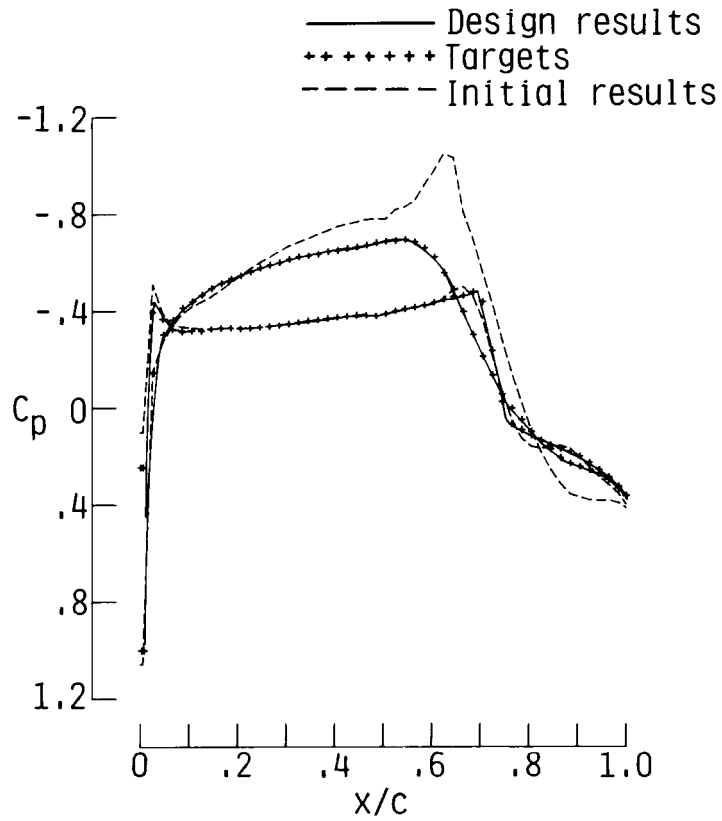

(a) Comparison of airfoil pressure distributions.

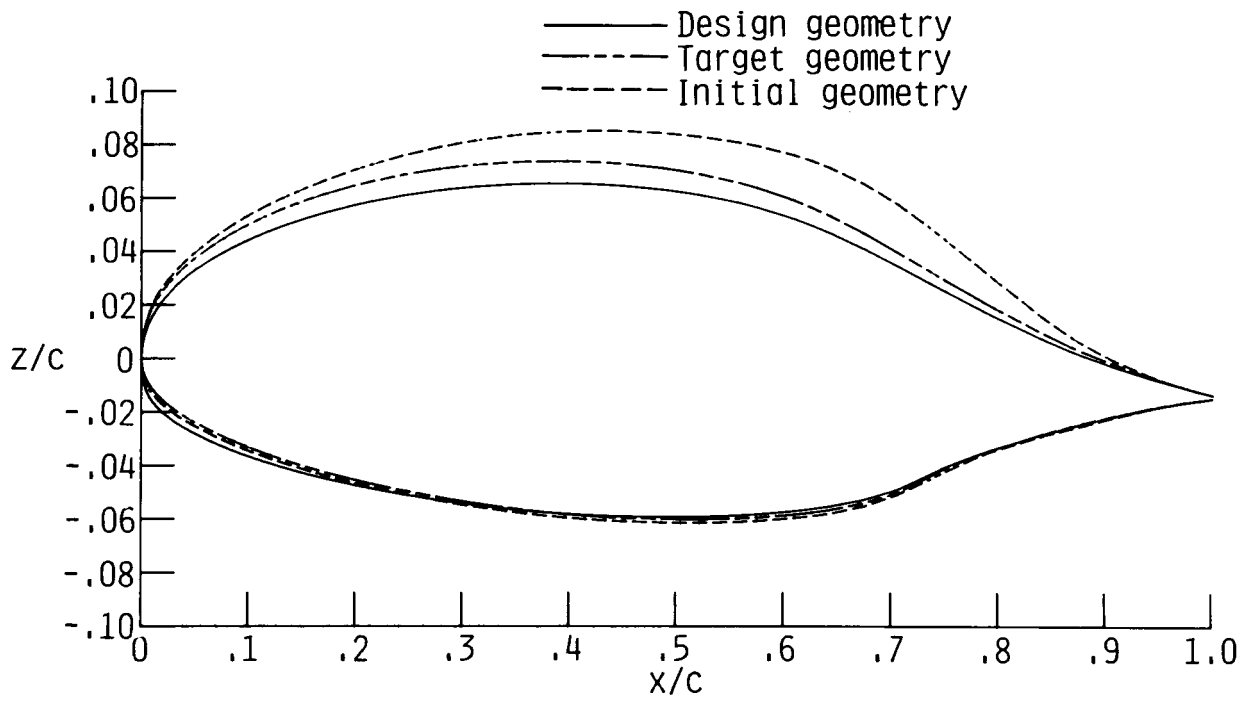

(b) Comparison of airfoil geometries.

Figure 15. Results for design case with modified 14-percent-thick airfoil as starting geometry at $M_\infty = 0.70$ and $\alpha = -0.193°$.

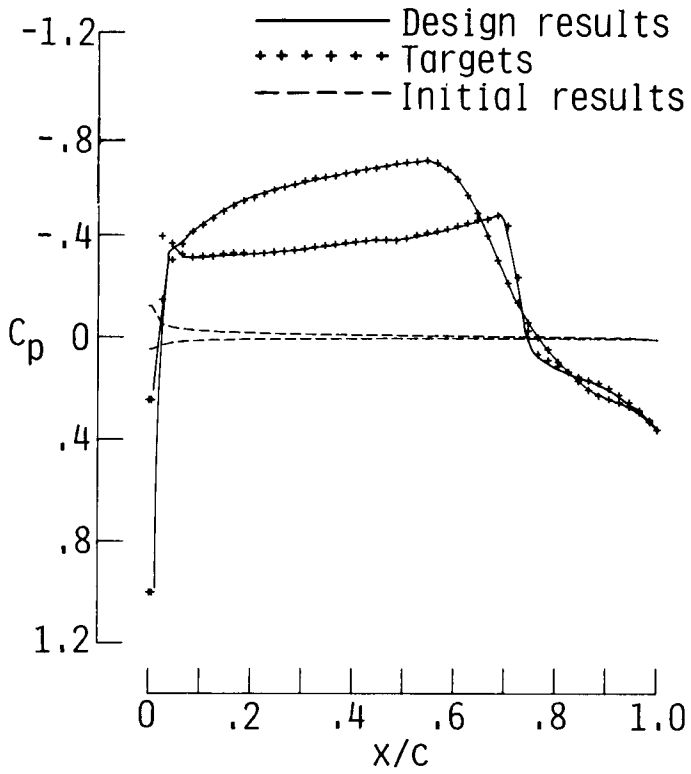

(a) Comparison of airfoil pressure distributions.

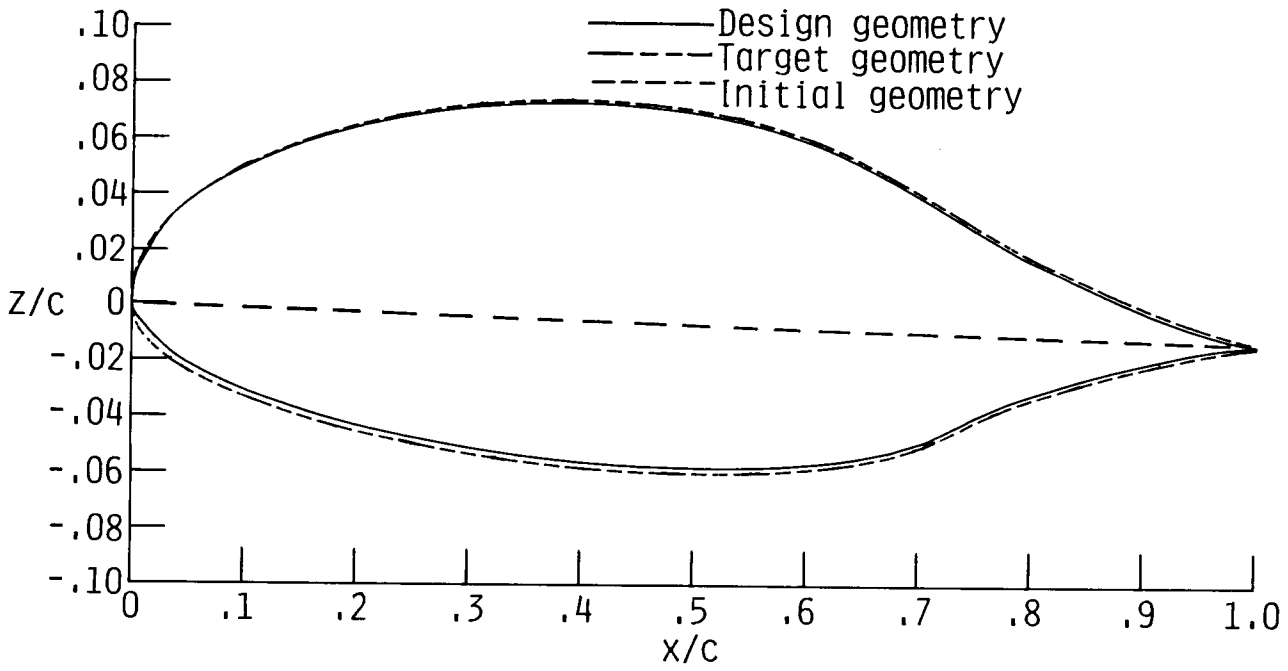

(b) Comparison of airfoil geometries.

Figure 16. Results for design case with modified 14-percent-thick airfoil as starting geometry at $M_\infty = 0.70$ and $\alpha = -0.193°$.

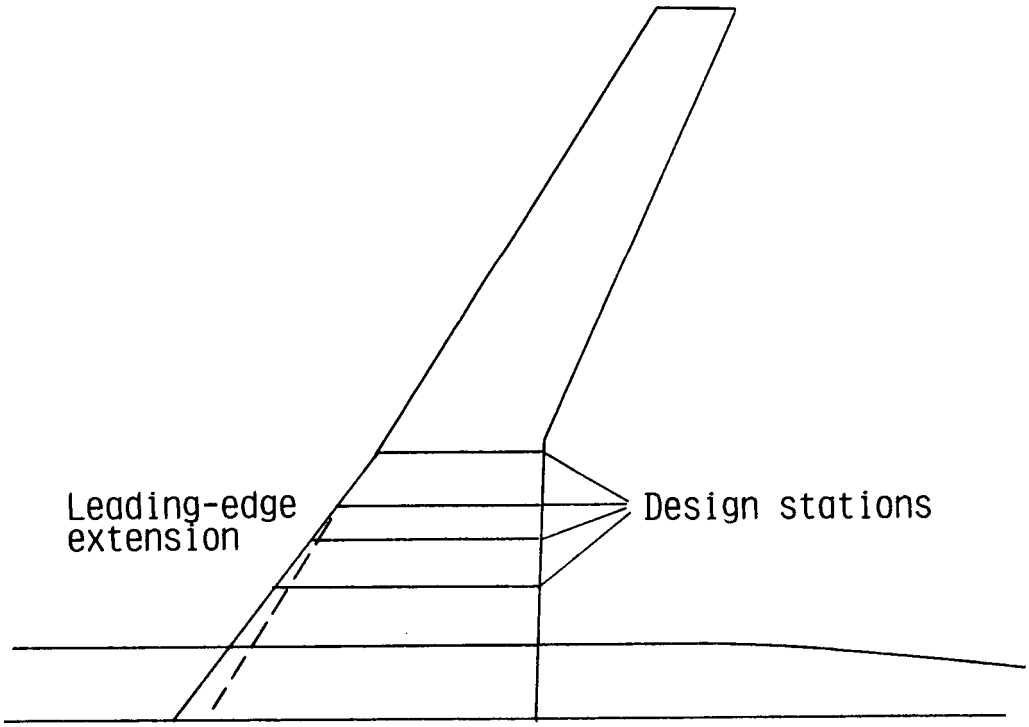

Figure 17. Planform definition for supercritical-wing design test case. Sweep = 30°; Aspect ratio = 9.8.

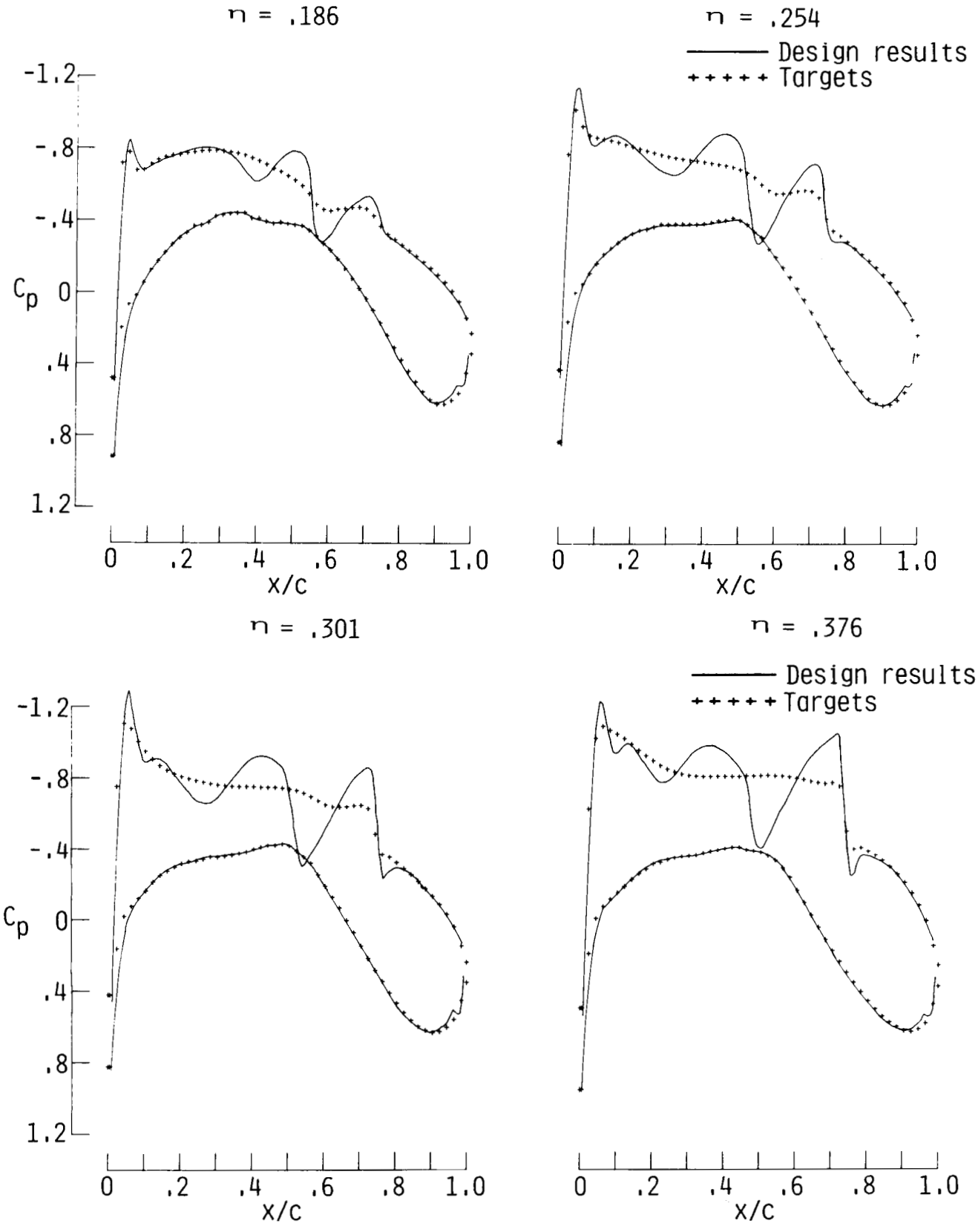

Figure 18. Results for design test case to duplicate supercritical-wing design at $M_\infty = 0.83$ and $\alpha = 2.19°$.

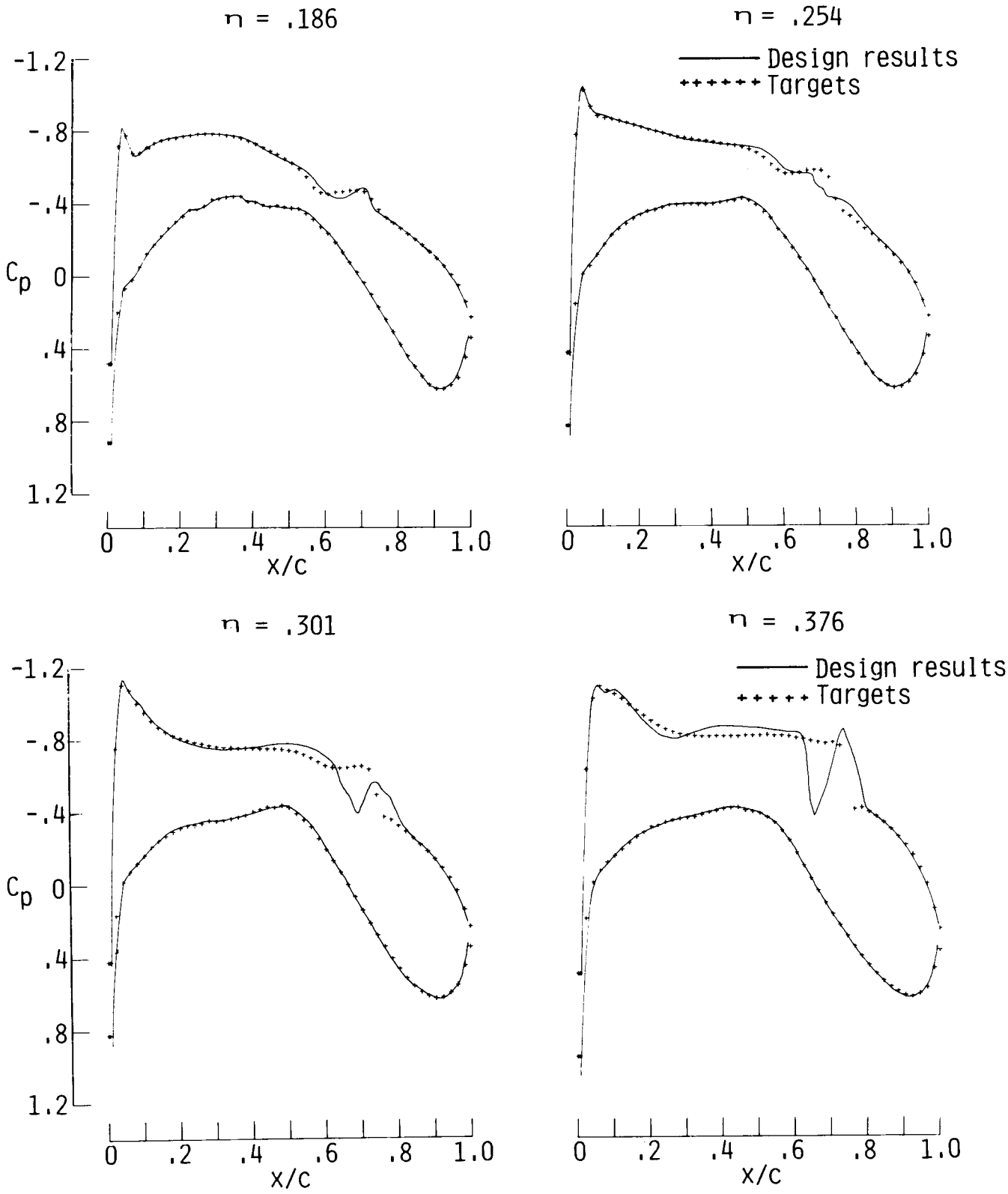

Figure 19. Results for design test case to duplicate supercritical-wing design at $M_\infty = 0.83$ and $\alpha = 2.19°$ after 100 design steps.

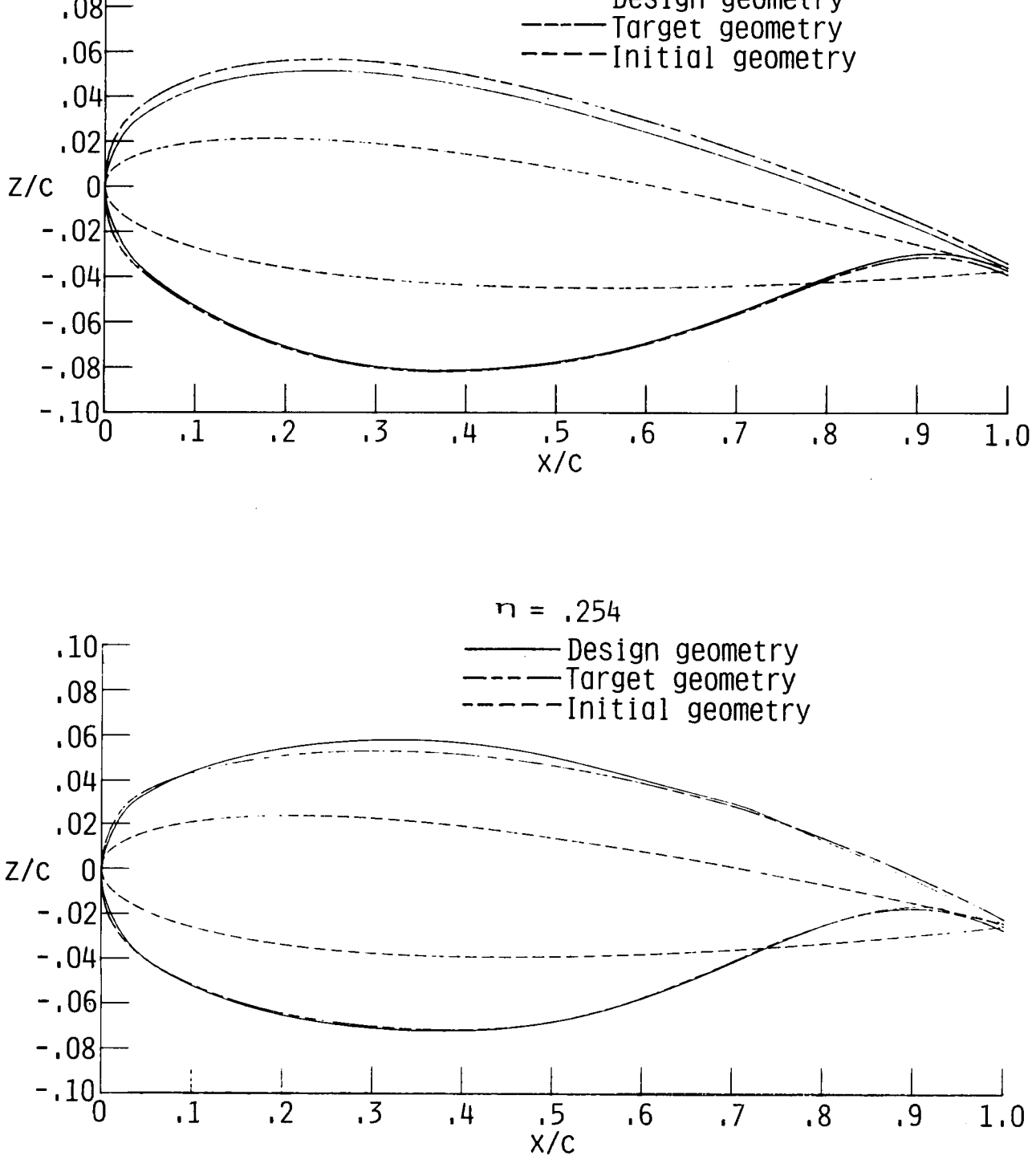

Figure 20. Comparison of design airfoils with target airfoils for supercritical-wing design test case.

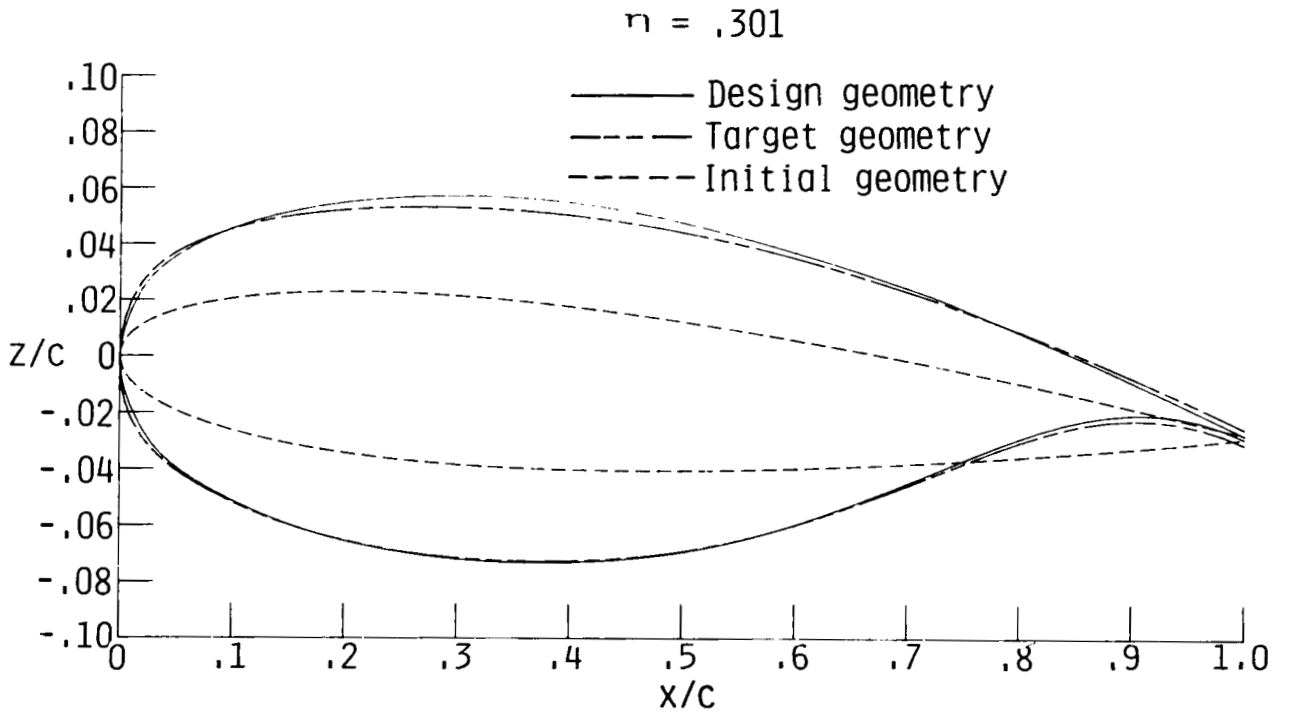

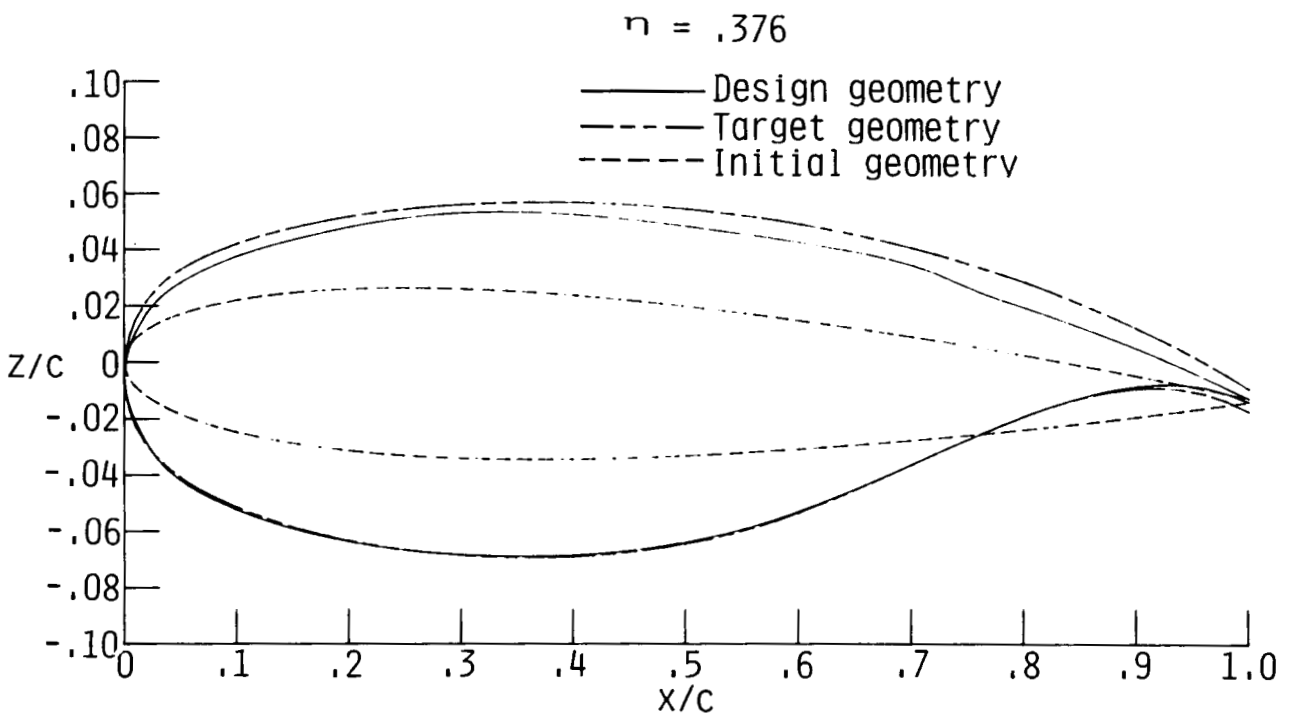

Figure 20. Concluded.

NASA
National Aeronautics and Space Administration

Report Documentation Page

1. Report No.	2. Government Accession No.	3. Recipient's Catalog No.
NASA TP-2806		

4. Title and Subtitle	5. Report Date
A Transonic-Small-Disturbance Wing Design Methodology	March 1988
	6. Performing Organization Code
7. Author(s)	8. Performing Organization Report No.
Pamela S. Phillips, Edgar G. Waggoner, and Richard L. Campbell	L-16393
9. Performing Organization Name and Address	10. Work Unit No.
NASA Langley Research Center Hampton, VA 23665-5225	505-60-21-02
	11. Contract or Grant No.
12. Sponsoring Agency Name and Address	13. Type of Report and Period Covered
National Aeronautics and Space Administration Washington, DC 20546-0001	Technical Paper
	14. Sponsoring Agency Code

15. Supplementary Notes

16. Abstract

An automated transonic design code has been developed which modifies an initial airfoil or wing in order to generate a specified pressure distribution. The design method uses an iterative approach that alternates between a potential-flow analysis and a design algorithm that relates changes in surface pressure to changes in geometry. The analysis code solves an extended small-disturbance potential-flow equation and can model a fuselage, pylons, nacelles, and a winglet in addition to the wing. A two-dimensional option is available for airfoil analysis and design. Several two- and three-dimensional test cases illustrate the capabilities of the design code.

17. Key Words (Suggested by Authors(s))
Transonic flow
Wing design
Airfoil design
Potential flow

18. Distribution Statement
Unclassified—Unlimited

Subject Category 02

19. Security Classif.(of this report)	20. Security Classif.(of this page)	21. No. of Pages	22. Price
Unclassified	Unclassified	29	A03

For sale by the National Technical Information Service, Springfield, Virginia 22161-2171